UPPSALA
UNIVERSITET

Digital Comprehensive Summaries of Uppsala Dissertations from the Faculty of Science and Technology 766

Characterization and Functionalization of 2D Overlayers Adsorbed on Transition Metals

MAY LING NG

ACTA
UNIVERSITATIS
UPSALIENSIS
UPPSALA
2010

ISSN 1651-6214
ISBN 978-91-554-7890-2
urn:nbn:se:uu:diva-130342

Dissertation presented at Uppsala University to be publicly examined in Room 80101, Ångström Laboratory, Lägerhyddsvägen 1, Uppsala, Friday, November 5, 2010 at 10:15 for the degree of Doctor of Philosophy. The examination will be conducted in English.

Abstract
Ng, M L. 2010. Characterization and Functionalization of 2D Overlayers Adsorbed on Transition Metals. Acta Universitatis Upsaliensis. *Digital Comprehensive Summaries of Uppsala Dissertations from the Faculty of Science and Technology* 766. 79 pp. Uppsala. ISBN 978-91-554-7890-2.

Two-dimensional layered materials, namely monolayer hexagonal boron nitride and graphene were grown by CVD on various transition metals. The physical and chemical properties of these systems were characterized systematically using synchrotron-based spectroscopic techniques, scanning tunneling microscopy and low energy electron diffraction. It is learned that the overlayer–substrate interaction is caused by the overlayer π–substrate d band hybridization. The physical properties of these overlayers depend on the strength of interaction and the degree of lattice matching at the interface. The strength of interaction between the boron nitride and graphene overlayers and the transition metal substrates is increasing from Pt(111)–Ir(111)–Rh(111)–Ru(0001). For overlayers adsorbed on Rh and Ru, the interplay between these two parameters can result in corrugation of the overlayer, i.e. a surface with bonding and non-bonding areas. The amplitude of corrugation is increasing with the strength of interfacial interaction. The corrugated BN overlayer (BN nanomesh) was used as a template for the growth of two-dimensional and highly dispersive Au nanoparticles. In addition, the inert BN nanomesh was used as a substrate for the deposition of pentacene molecules that conform to the corrugated surface while preserving the herringbone crystal structure. The coadsorption of oxygen and Co clusters on the nanomesh was investigated. Oxygen was utilized to lower the Co surface energy, i.e. to prevent Co agglomeration. It is observed that the smaller Co clusters intercalate through the BN overlayer upon soft annealing. Beside the surface structure, the substrate induced surface reactivity of the MG overlayer was employed to promote the hydrogenation of graphene on Pt, Ir and Ni. The graphene layer adsorbed on Pt and Ir shows higher H uptake than MG/Ni. Furthermore the uptake increases with the size of the bonded graphene. The small H uptake for MG/Ni was attributed to the electron localization in the C-Ni bonds.

Keywords: h-BN, graphene, transition metals, nanomesh, functionalization, PES, NEXAFS, STM, LEED

May Ling Ng, Department of Physics and Astronomy, Surface and Interface Science, 516, Uppsala University, SE-751 20 Uppsala, Sweden

ISSN 1651-6214
ISBN 978-91-554-7890-2
urn:nbn:se:uu:diva-130342 (http://urn.kb.se/resolve?urn=urn:nbn:se:uu:diva-130342)

Till gubben och plutten

List of Papers

This thesis is based on the following papers, which are referred to in the text by their Roman numerals.

I **Influence of chemical interaction at the lattice-mismatched h-BN/Rh(111) and h-BN/Pt(111) interfaces on the overlayer morphology**
A. B. Preobrajenski, A. S. Vinogradov, M. L. Ng, E. Ćavar, R. Westerström, A. Mikkelsen, E. Lundgren, N. Mårtensson
Physical Review B 75, 245412 (2007)

II **Monolayer h-BN on lattice-mismatched metal surfaces: On the formation of the nanomesh**
A. B. Preobrajenski, M. A. Nesterov, M. L. Ng, A. S. Vinogradov, N. Mårtensson
Chemical Physics Letters 446 (2007) 119–123

III **Adsorption-induced gap states of h-BN on metal surfaces**
A. B. Preobrajenski, S. A. Krasnikov, A. S. Vinogradov, M. L. Ng, T. Käämbre, A. A. Cafolla, N. Mårtensson
Physical Review B 77, 085421 (2008)

IV **Formation and temperature evolution of Au nanoparticles supported on the h-BN nanomesh**
M. L. Ng, A. B. Preobrajenski, A. S. Vinogradov, N. Mårtensson
Surface Science 602 (2008) 1250–1255

V **A single h-BN layer on Pt(111)**
E. Ćavar, R. Westerström, A. Mikkelsen, E. Lundgren, A.S. Vinogradov, M. L. Ng, A. B. Preobrajenski, A. A. Zakharov, N. Mårtensson
Surface Science 602 (2008) 1722–1726

VI **Controlling graphene corrugation on lattice-mismatched substrates**
A. B. Preobrajenski, M. L. Ng, A. S. Vinogradov, N. Mårtensson
Physical Review B 78, 073401 (2008)

VII **Impact of oxygen coadsorption on intercalation of cobalt under the h-BN nanomesh**
A. B. Preobrajenski, M. L. Ng, N. A. Vinogradov, A. S. Vinogradov, E. Lundgren, A. Mikkelsen, N. Mårtensson
Nano Letters Vol. 8, No. 7, 2009

VIII **Effect of substrate nanopatterning on the growth and structure of pentacene film**
M. L. Ng, A. B. Preobrajenski, A. A. Zakharov, A. S. Vinogradov, S. A. Krasnikov, A. A. Cafolla, N. Mårtensson
Physical Review B 81, 115449 (2010)

IX **Controlling hydrogenation of graphene on transition metals**
M. L. Ng, R. Balog, L. Hornekær, A. B. Preobrajenski, N. A. Vinogradov, N. Mårtensson, K. Schulte
Accepted in Journal of Physical Chemistry C

I have contributed to the experimental results in the following paper that is not included in this thesis.

I **Dynamical effects in x-ray absorption spectra of graphene and monolayered h-BN on Ni(111)**
J. Rusz, A. B. Preobrajenski, M. L. Ng, N. A. Vinogradov, N. Mårtensson, O. Wessely, B. Sanyal, O. Eriksson
Physical Review B 81, 073402 (2010)

Comment on my own participation
I have made contributions to all included papers. My position in the author lists reflects the amount of work on the respective paper, which has been my responsibility. In the case that I have the first position in the author list, I have had the main responsibility for the paper.

Contents

1. Introduction

Surface science is a fascinating and intriguing field of studies because it never ceases to amaze us with inspiring and serendipitous discoveries that may contribute to our understanding of fundamental sciences. The route to obtaining any results from surface studies is often an adventurous odyssey due to the stringent preparation and measurement environment and complicated data analysis procedures. A remarkable example is the seemingly simple reaction between nitrogen and hydrogen to produce ammonia. It has demanded a tedious 60-year time to fully understand the process, whereby Gerhard Ertl was honored the Nobel Prize in Chemistry in 2007 for unraveling the Haber-Bosch process. Undoubtedly, the informative results attained from surface studies are worth the endeavor.

In this thesis, two dimensional (2D) layered materials are the focus of studies because they have very interesting electronic and structural properties. For 2D systems, electrons are quantized in one spatial dimension but are free to travel in the other two dimensions, i.e. in-plane. [1] This confines the electron propagation in the plane that is only a single atom thick. Despite the monoatomic thickness, these 2D materials have superior mechanical stability due to the strong intra-molecular covalent bonds in the basal plane.

Monolayer (ML) hexagonal boron nitride (h-BN) is a classical example of a 2D layered material with strongly anisotropic chemical bonds, which is isostructural to graphene. [2, 3]. Conventionally, h-BN films are used as anti-corrosive and oxidation resistant coatings. [4] It has been discovered that h-BN forms a continuous single monolayer on Pt(111) and Ru(0001) surfaces, as interpreted from the coincident electron diffraction patterns. [5] Later, Nagashima and co-workers [6] investigated the electronic structures of the h-BN ML grown on Ni, Pd and Pt(111). They have discovered that h-BN is bound slightly stronger on Ni than on Pd and Pt. This statement is further strengthened by the phonon spectra measured by Rokuta *et al.* in Ref. [7]. In 2004, it was observed by scanning tunneling microscopy that the h-BN overlayer adsorbed on Rh(111) inherited highly regular hexagonal hole and wire structures, which is regarded as the BN nanomesh [8]. Preobrajenski *et al.* [9] have investigated the role of the TM d-band and h-BN π-band hybridization for the formation of the h-BN/Ni(111) interface. It is apparent that the electronic structure of a single ML of h-BN adsorbed on Ni(111) is strongly modified due to hybridization. In addition, it is shown that the ML is flat and continuous. In a subsequent paper [10], the strength of the h-BN–TM

interaction is associated with the TM $3d$-band electronic configuration by comparing the adsorption of h-BN on Cu(111) (fully occupied $3d^{10}$) with that on Ni(111) ($3d^9$). It is found that h-BN grows easier on Ni than Cu. There is also a substantial $d-\pi$ hybridization upon adsorption on Ni, which is not observed for the Cu case. Thereby it is concluded that h-BN is chemisorbed on Ni but weakly physisorbed on Cu.

In contrast to the insulating h-BN, graphene or monolayer graphite (MG)[1] is a superb conductor with ballistic electron transport [11, 12]. Similar to h-BN, MG may also form a continuous monolayer [13] on reactive transition metals (TMs) surfaces independent of the substrate atomic scale imperfections (surface roughness and steps), i.e. it can grow over an atomic step as a continuous monolayer. [14]. Besides, MG on TM is a remarkable system due to the vast possibility to manipulate the electronic and magnetic properties of graphene by chemical adsorption.

1.1 The Motivation

Due to the continuity of h-BN [5] and MG [11] single atomic layer on TM substrates, they can be viewed as a 2D macromolecule. The in-plane bonds are strong due to the sp^2 hydridization while the interaction with the substrate is weaker. Depending on the degree of orbital mixing between the overlayer π and TM d electrons, these overlayers have different strength of interfacial interaction with the substrates. [2] As a consequence, the adsorbed overlayers have different surface structures as well as chemical reactivities on different TM surfaces. Thence, a thorough understanding of the relation between interaction strength and morphology is the key to tailoring the h-BN and graphene electronic properties specific to their application [15, 16]. Moreover, these systems can play the role of a pristine physical as well as chemical template for further functionalization by metal and molecule adsorption. [14, 17, 18] Outstanding properties, such as catalytic function, not found in the bulk can be expected in the template-supported metal nanoparticles. [19, 20] Both template structure and chemical reactivity are unique to the type of overlayer and TM substrate because they are controlled by the interfacial interaction and lattice matching. Therefore, it is fundamentally as well as technologically important to study the adsorption trends of h-BN and MG on TM surfaces with various atomic and electronic structures.

[1] Owing to the diverse definitions of graphene, it is important to clarify here that graphene or MG, whenever it is mentioned in this thesis, means a *single* monolayer (ML) of graphite. Otherwise, the number of MLs will be explicitly specified.

1.2 The Objectives

The goal of this work is to undertake systematic and comparative studies of the nature and strength of interfacial interaction between MG and h-BN overlayers and TMs using synchrotron-based surface science methods, namely photoelectron spectroscopy (PES), near edge absorption fine structure (NEXAFS) and x-ray emission spectroscopy (XES). Combining the spectroscopic measurements with low energy electron diffraction (LEED), low energy electron microscopy (LEEM) and scanning tunneling microscopy (STM), it is possible to explain the nature of interfacial bonding as well as to map the morphology of these overlayers. To achieve these, the experiments are subtly designed to reveal and establish the general trends of the overlayer–substrate bond strength by adsorption of h-BN respective MG on TM surfaces with different electronic structure of the nd-shell ($n = 3,4,5$). Succeedingly, the h-BN systems are surface functionalized with monodispersed gold nanoparticles, intercalated cobalt clusters and ordered monolayer of pentacene while the MG systems are exposed to atomic hydrogen.

1.3 Adsorption of Overlayers on Surfaces

The study of fundamental properties of adsorbed materials on solid surfaces is very important in the quest for novel properties in materials. In this dissertation, transition metals are chosen as the substrates because they are relatively reactive due to the partially filled d-sub shells. This makes them an attractive "playground" for depositing adsorbates and to study both the resultant interfacial interaction as well as the microscopic surface structure and macroscopic morphology.

1.3.1 Dynamics of Adsorption

When a clean surface is exposed to atoms or molecules (hereafter referred to as particles for simplicity) in the ultra high vacuum (UHV) environment, collisions between the incident particles and the surface take place. Depending on the details of the interaction between the particles and surface, the particles will either reside on the surface or be back-reflected into the vacuum. If the trapping potential is not very strong, the particles are capable to diffuse along the surface. The residence time of the particles is determined by the kinetic energy of the particles and the surface energy. In addition, molecules may exchange their internal energies with the surface. If they possess enough kinetic energy to overcome the adsorption energy, they will desorb from the surface in gas phase. Desorption may occur directly or via different dynamic processes such as dissociative and associative desorption [21, 22]. In dissociative desorption, the incoming molecules are cracked at the substrate surface, which become smaller fractions prior

to desorption. On the other hand, the incoming species may react with the adsorbates on the substrate forming a gaseous phase of the species in associative desorption, e.g. the Eley-Rideal mechanism [22, 23].

Physical barriers such as defects and step edges may also affect the adsorption rate. These structural imperfections impose a barrier for the adsorbate diffusion, thus increasing the nucleation density. In fact, the heat of adsorption is typically higher at the defected site, step edge and kink than at the terrace of a single crystal substrate surface. This is explained by the attempt of surface electrons to even out the abrupt discontinuity at such imperfections by spilling out the charges from the surface, which is also known as Smoluchowski smoothing [24]. Therefore, surface reactivity is typically stronger at these sites as compared to the terraces. [21]

At thermodynamical equilibrium, particles adsorb in the energetically favorable sites, i.e. the sites of high binding energy, and may become nuclei for island growth. Eventually, the island grows larger and merges with neighboring islands to form an overlayer.

1.3.2 Types of Adsorption

For the gas-solid interfaces in an ideal situation, it is common to use the Langmuir model to describe the adsorption process. This model describes the adsorption of a ML of an ideal gas onto an idealized surface. In reality many other factors have to be incorporated into the model in order to estimate the process more accurately, such as interaction between the adjacent adsorbates (associative adsorption), competition between adsorption and desorption processes, dissociation of the molecules upon adsorption and so forth.

Basically, the adsorption of a ML on a surface is governed by two simple parameters, namely the interaction between the adsorbates and between the adsorbate and the surface. For the sp^2 materials on TM surfaces, a slight difference in the electronic configuration of the adsorbate π band and/or substrate d band may result in detectable changes in the adsorbate-adsorbate and adsorbate-substrate interaction.

There are two types of inter-adsorbate interactions during adsorption, i.e. adsorbate association and dissociation. For associative adsorption, the adsorbates attach to the substrate surface and simultaneously, translate on the surface to find and bond with each other to form larger molecules, i.e. the Langmuir-Hinshelwood mechanism [21, 22, 23]. The dissociative adsorption process is not relevant to this work and therefore it will not be discussed further.

A special case of associative adsorption is the organization of adsorbed particles into a 2D macromolecule during adsorption. First, the precursor molecules adsorb on the hot surface and are catalytically fragmented. There fragments gradually form an ordered ML solely in the government of the inter-molecular interaction. This autonomous process is also known as self-assembly of a monolayer [25, 26]. In fact, the self-assembly

of a monolayer is the foundation of this work. A major effort has been dedicated to characterize the catalyzed dehydrogenation of borazine (hydrocarbon) molecules and the assembly of B and N (C) atoms into epitaxial h-BN (graphene) monolayers on TM surfaces. In addition to the inter-molecular interaction that forms the continuous ML, the interplay between the adsorbate-substrate interaction and the lattice parameters determine the ML surface morphology.

Therefore, the adsorption process for the organized overlayers can be further classified according to the strength of adsorbate-substrate interaction, i.e. physisorption and chemisorption. Physisorption is a process in which the electronic structure of the adsorbate is barely perturbed upon adsorption. When a particle approaches a surface, it senses an attractive potential correlating to charge polarization (no charge transfer) in the interface, i.e. between the mutually induced dipole moments. This weak interaction is known as van der Waals force or "fluctuating dipole" in molecular physics. For physisorbed adlayer, the adsorbate-adsorbate interaction usually dominates the adsorbate-substrate one. An example of this case is the adsorption of molecules on TM with almost or fully occupied *d*-band, where the covalent bonds between adsorbed species is stronger than the weak adsorbate-TM interaction.

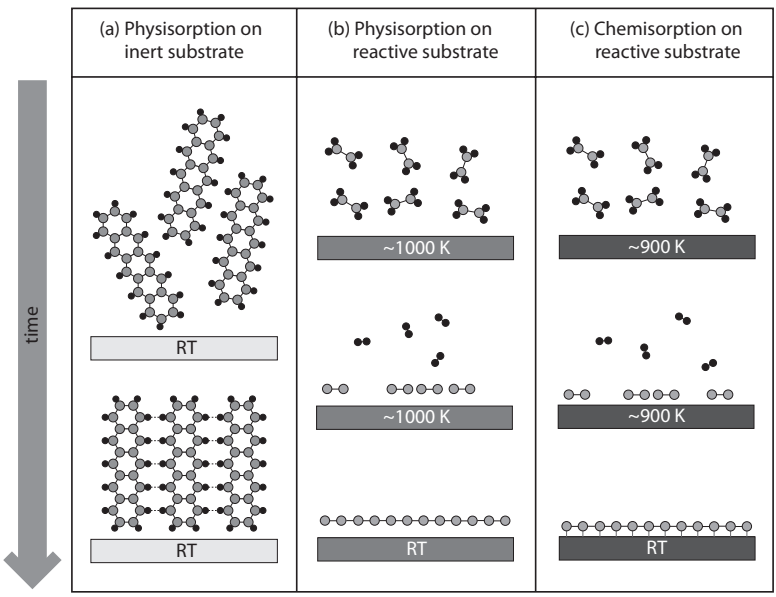

Figure 1.1: Schematics of various types of associative adsorption processes to form a continuous monolayer, namely (a) physisorption on inert surface, e.g. pentacene on BN/TM, (b) physisorption on reactive substrate, e.g. ethene on Ir(111) and (c) chemisorption on reactive substrate, e.g. ethene on Ni(111).

For associative physisorption of admolecules on inert surfaces, these molecules remain intact, i.e. neither broken nor distorted. Since the molecule-substrate interaction is rather weak, they can re-arrange

themselves into their natural crystalline structure via weak intra-molecular interaction such as van der Waals and hydrogen bonds, as illustrated in Fig. 1.1(a). This process is exemplified by the work published in Paper VIII, where pentacene molecules are weakly adsorbed on the non-reactive BN nanomesh. On more reactive transition metal surfaces, the adsorbates can also re-establish their intra-molecule bonds. For example, unsaturated hydrocarbon molecules, e.g. ethene and propene are catalytically dehydrogenated on TM surfaces. Subsequently, the cracked molecules diffuse on the substrate until they find suitable adsorption sites. These adsorbates are now the nucleation seeds for the incoming cracked molecules, where they can form larger network of molecules, i.e. a 2D macromolecule via covalent bonds as shown in Fig. 1.1(b). However, the adsorbate–substrate interaction is weak, i.e. there is no new hybrid states formed in the interface.

In chemisorption, an interaction between the adsorbate and the reactive metal substrate is established because two orbitals with suitable symmetry and radial distribution form a common bonding orbital. Here, an electron exchange between the adsorbate and the metal can occur. As a result, these electrons are shared between the adsorbate and the metal forming the hybridized orbital. Chemisorption resembles the formation of covalent or ionic bonds, where the adsorbate–substrate electronic structure is heavily perturbed and new hybrid states are developed. For instance, when a molecule with partially filled π orbital approaches a reactive TM surface with partially filled d-band, these orbitals overlap and rehybridize to form a new orbital. Owing to the nature of bonding, chemisorbed species can be characterized by their high binding energies and short equilibrium bond lengths (see Fig. 1.1(c)). The adsorbate-substrate interaction may have some impact on the overlayer such as weakening of the interatomic bonds and altering of the overlayer surface structure.

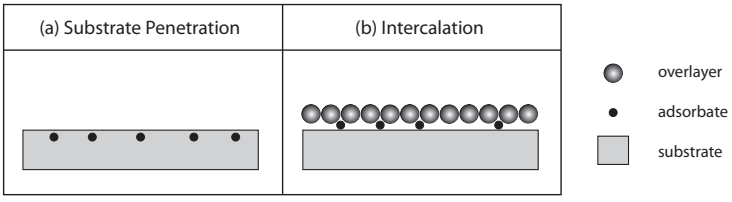

Figure 1.2: Schematics of other adsorbate–substrate interactions, namely (a) substrate penetration and (b) intercalation.

Instead of forming islands on top of a solid surface, adatoms can diffuse and penetrate into a reactive metal surface due to the very strong mutual interaction. At low concentrations, these adatoms sit sparsely in the interstitial positions of the metal lattice. With increasing amount of adatoms on the metal surface, surface metal compounds may be formed, e.g. borides [27], carbides [28] and oxides [29, 30, 31]) for organic adsorbates. In the case

of metal adatoms, surface alloys [32] may form in the topmost layers of the metal substrate, as shown in Fig. 1.2(a).

For metal surfaces covered with an overlayer, energetic or reactive adatoms can still reach the underlying metal surfaces by intercalation via the defected sites and the edges of the overlayer. [14] These adatoms may gradually penetrate further into the metal substrate as described previously or simply reside between the overlayer and the metal surface, as depicted in Fig. 1.2(b).

1.3.3 Growth Modes

Under suitable conditions, the adsorbate nucleation seeds on the substrate will eventually form an overlayer or a film. On solid surfaces there are three main modes of the thin film growth, namely layer-by-layer (Frank-van der Merwe, FM), island (Vollmer-Weber, VW) and layer plus island (Stranski-Krastanov, SK) growth mode (see Fig. 1.3).

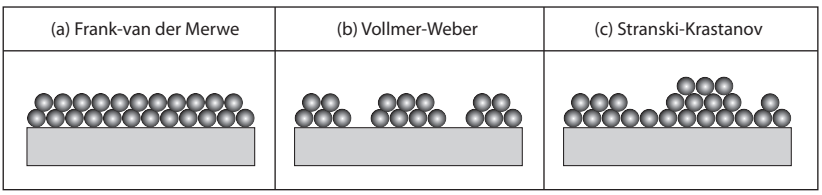

Figure 1.3: Three modes of overlayer growth, namely (a) Frank-van der Merwe, (b) Vollmer-Weber and (c) Stranski-Krastanov.

According to Bauer and Poppa [33], the growth modes are determined by the surface energies of the overlayer and the substrate. The film grows in either the FM or SK mode when the surface energy of the substrate is higher than that of the overlayer. If the surface energy of the film is higher than its strain energy, it will grow in the FM mode. Vice versa for the SK mode. The VW mode occurs when the surface energy of the overlayer is larger than that of the substrate. However, these general rules are only valid if there is no chemical reactions during the adsorption process. Agile and Rhead [34] also stated that the validity depends on the local surface equilibrium, namely the surface diffusion rate must be higher than the vapor impingement rate. Conversely, the growth rate has to be low.

In the FM mode, adsorbates attach to the energetically favorable sites on the substrate to reduce the surface free energy. As a result, nucleation centers are formed. Now, the following incoming particles are diffusion limited by the existing nucleation centers. Depending on the precursor type, the diffusion mechanism can be explained by two different models. For intrinsic precursors (those residing above a vacant site), diffusion-limited aggregation (DLA) is used to describe the adsorption mechanism. In this model, the precursor is assumed to walk on the substrate surface until it finds a nucleation center and merges with it [35, 36]. Meanwhile, the adsorption of

extrinsic precursors is modeled by diffusion-limited island growth (DLIG) [37], i.e. the precursor arrives on top of an existing island and migrates to the edge of the island to incorporate to the islands. DLA results in dendritic structures while DLIG gives more rounded islands.

In fact, there is another type of 2D growth mode that is similar to the FM mode but the maximum amount of adsorbate is limited by the active sites on the substrate, i.e. not exceeding 1 ML. This is known as the substrate activated growth, where the substrate first acts as the catalyst for the decomposition of the adsorbates that later adsorb on the substrate. The growth is terminated upon full coverage of the substrate surface. This is because the process has high activation energy, which needs the assistance of a catalyst to proceed. When all the catalytic sites are fully occupied, the substrate is instantaneously deactivated [38, 39]. As a result, this adsorption process is self-limiting at a given temperature, i.e. only a monolayer of adsorbates at the maximum can be accommodated on the substrate surface.

SK mode is the intermediate growth mode that is similar to the FM mode. First, the adsorbate attach to the substrate and grow as a 2D layer for the first ML and up to a few MLs. However, the growth is disrupted when the balance of forces changes due a mismatch in the lattices. This mismatch causes an accumulation of strain in the growing layer, which results in the change from a 2D epitaxial to 3D crystallite growth mode.

1.3.4 Ordered Monolayers

In this work, only ordered monolayers are considered because their properties are more predictable and uniform over a long range. This exerts control over the growth, which ensures reproducibility and suggests possibilities for functionalization. Furthermore, the ambiguity of the experimental result interpretation is profoundly reduced with ordering.

The ordered surface of crystals with cubic lattices are commonly represented by the Miller indices, (hkl) or Miller-Bravais indices, (hkil). Throughout this thesis, only the hexagonal close-packed, hcp(0001) and face-centered cubic, fcc(111) substrate surfaces are used (see Fig. 1.4). They have the well defined and tightly packed atomic coordination. Therefore, surface relaxation as well as adsorption induced surface restructuring are at the minimum.

During adsorption, the adlayer is reconstructed in order to accommodate the adsorbates on the substrate at the energetic optimum. In practice, the reconstruction can be characterized with LEED that shows the overlayer superlattice/superstructure relative to the (1×1) substrate lattice, in terms of the unit cell vectors in reciprocal space.

There are two ways of defining a ML according to Ref. [41], namely lattice-saturated ML and geometric ML. The lattice saturated ML is formed when all accessible sites on the substrate surface lattice are occupied by adsorbates, i.e. the amount of adspecies depends on the number of favorable adsorption sites. Hence, the driving force for the formation of this ML is

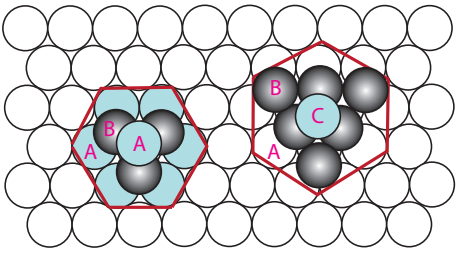

Figure 1.4: [left] hcp with AA stacking (Bernal) and [right] fcc lattice with ABC stacking (rhombohedral). *Reproduced based the original in [40].*

mainly the adsorbate-substrate interaction. The geometric ML is defined as a layer of single atomic or molecular thick, close packed adsorbates of finite size. Here, the amount of adspecies varies with the packing ability of the particles on the substrate, i.e. the closer they arrange themselves on the surface, the more material is adsorbed. There is a profound difference in the amount of adsorbates for a geometric ML for large or elongated molecules such as pentacene. For example, the amount of C in a geometric ML of standing-up pentacene is much higher than a ML of lying-down ones. In this case, both the adsorbate-adsorbate and absorbate-substrate interactions may influence the adsorption process. Therefore the amount of standing and lying pentacene adsorbed on the h-BN nanomesh in this work is determined by calibrating the C 1*s* photoemission intensity of these samples to the one from a ML of flat graphene adsorbed on Rh(111). A ML of graphene is assumed as the densest configuration for the flat-lying pentacene. Since the packing density of all three samples are known, the intensity of the C 1*s* signal can be easily transformed into the amount of C atoms in terms of standing respective lying ML.

1.4 Functionalization of Adsorbed Overlayers

In principle, all micro- and nanofabrication methods can be branched into two general groups, i.e. top down (lithographic techniques) and bottom up (self-assembly). Self-assembly is a relatively new method as compared to its mature and limit-approaching lithographic counterpart. The idea of exploiting self-assembly was already born on 29 December 1959, the day Richard Feynman presented his classical talk entitled "*There's plenty of room at the bottom*". [42] Self-assembly is practically an imitation of the nature where molecules/atoms are the building blocks and the process is governed by the feasibility of their mutual interaction. The replication of complicated DNA helix from very specific bonding between protein molecules is an example of self assembly from the nature.

1.4.1 Nanotemplating

Intuitively, when the self-assembly process itself is highly repetitive, specific and well-ordered down to the nanometer scale, it is very alluring to employ this fast and accurate process to produce nanotemplates. The idea of nanotemplating is to employ the uniformly patterned structures as physical traps for subsequent arrangement of metals or molecules into arrays of nanoparticles or crystalline overlayers. The ordered and monodispersed nanoparticles can in turn be functionalized with biomolecules or proteins. In addition, metal nanoparticles are known to have enhanced quantum physical properties not exhibited in macroscopic scale. This is important in many technological applications such as catalysis, magnetic data storage, gas sensors, organic electronics, etc. In addition to the trapping function, the nanotemplate can also be used to re-shape the crystal lattice of an overlayer adsorbed on the template. This is provided that the template is not strongly reacting with the overlayer, which preserves the overlayer crystallinity.

1.4.2 Controlled Intercalation

Intercalation of metal atoms with low ionization potential in an adsorbed overlayer takes place readily while the intercalation of other atoms with high ionization potential can be induced thermally and even chemically. Studies show that the intercalation of Cs, K and Na in graphene on Ir(111) occurs between 300–400 K while intercalation of atoms with high ionization potential such as Pt, Ni and Mo starts at 1000 K. [43] As a consequence of intercalation, the electronic structure of the overlayer can be altered. Nagashima *et al.* [44] have measured the band structure changes induced by Cs, K and Na intercalation in MG on Ni(111). They have shown that it is favorable for the intercalants to occupy the interface region at the same time dilating the MG-Ni bond distance. This subsequently changes the electronic and structural properties of the MG layer that is originally bonded to Ni. Upon intercalation, the overlayer becomes nearly free-standing and can be n- or p-doped by the intercalants, which can cause a change of the surface work function [45]. Intercalation induced work function change [44, 14, 46] is very convenient for fine-tuning a band gap, which is highly relevant for technological applications, e.g. field effect transistors.

Beside thermally controlled intercalation, the process may also be controlled chemically. Metal adsorbates with very high surface free energy tend to agglomerate into large clusters to lower their surface energy. A comprehensive summary of metal surface energies is presented in [47]. Tölkes and co-workers [48] have studied the influence of co-adsorbed O_2 molecules on Co growing on the Cu(110) surface. According to the authors, oxygen acts as a surfactant that lowers the adsorbate surface energy and consequently, encourages the metal to grow epitaxially. In other words, O_2 wets and prevents

the "snowballing" effect of the Co clusters, which may help Co to intercalate under MG or h-BN monolayers on TM surfaces in the form of small 2D clusters.

1.4.3 Substrate Catalyzed Reaction

According to Svante Arrhenius (1859-1927), Nobel laureate in Chemistry in 1903, a chemical process is feasible at a certain temperature if the reactants have overcome the reaction activation energy. However, this activation energy can be lowered by a catalyst, i.e. a substance that lowers the activation energy of a chemical process without being consumed or altered itself. This principle is applied in the chemical vapor deposition (CVD) of thin films on reactive substrates. However, the efficiency of a substrate catalyst can be inhibited by the coverage or adsorption of the secondary product/byproduct from the catalytic process. As a result, the affected catalyst is deactivated.

Transition metals are typical catalysts for redox processes such as hydrogenation, oxidation, amination, etc. For example, Heintz and Parker [49], who have studied the activation energy for the oxidation of graphite in air, propose that the TM d-bands act as the acceptor of the graphite π-electron. In this way, the TM activates the oxidation of graphite. Bonzel and Krebs [50] studied the hydrogenation of molecular CO adsorbed on TM, where H_2 and CO adsorb dissociatively on the TM surface that acts as the catalyst. By applying the same principles to sp^2-bonded overlayers adsorbed on TMs, it is anticipated that the TM substrate can act as a catalyst for chemical interaction occurring on the overlayer. The substrate catalyzed reaction opens up a door to various chemical functionalizations of the sp^2-bonded overlayers adsorbed on TMs, which is much less feasible on the free-standing monolayers under realistic experimental conditions.

2. Electronic Structures

The detailed knowledge of the electronic structure of a system is the foundation for understanding surface and interface properties. The electronic structure of a material is ultimately determined by the electron-electron and electron-nucleus interactions under the subjection of the quantum mechanical laws. [51, 52, 53]

All electronic properties are principally generated from the interaction between the valence electrons. In an elemental semiconductor such as Si and Ge, a band gap separates the valence band (VB) from the conduction band (CB) that constitutes the unoccupied states. The Fermi level (highest occupied state) is located in the band gap. The chemical bonds in these materials are purely covalent with sp^3 hybridization. The VBs in semiconducting compounds are more complicated than in pure elements. [54] For example, the III-V semiconductors such as GaAs and AlAs have predominantly covalent bonds but some charge transfer between the elements may occur. This is due to the lower symmetry (as compared to elemental semiconductors) in these compounds. The charge transfer causes the ionic character in the bonds, which weakens the sp^3 hybridization. As a consequence, the single *s*-orbital at the bottom of the VB splits away from the three *p*-orbitals.

In metals, the VB and CB are overlapped and there is a high concentration of nearly free electrons at the surface, which spills out from the surface into the vacuum as exponentially decaying space charge. These surface electrons create an electric dipole on the surface, which is responsible for the relatively high work function on metal surfaces. By definition, the work function, ϕ of a material is the minimum energy required to liberate a valence electron from a solid surface into the vacuum with zero kinetic energy. Conversely, this is the energy difference between the Fermi level and the vacuum level.

There are many ways to construe a wealth of information from the electronic structure of a surface. The band structure of a crystal or a crystalline surface represents the dispersion relations of the valence band energies with respect to the **k**-space of the first Brillouin zone (BZ). The BZ is represented by the Wigner-Seitz cell in the reciprocal lattice. The high symmetry points and directions in face-centered cubic and hexagonal BZ are depicted in Fig. 2.1. The electron band dispersion in a periodic crystal lattice is a function of the **k**-vector. **k** is the Bloch plane wave vector that describes the Bloch wave function in a periodic potential.

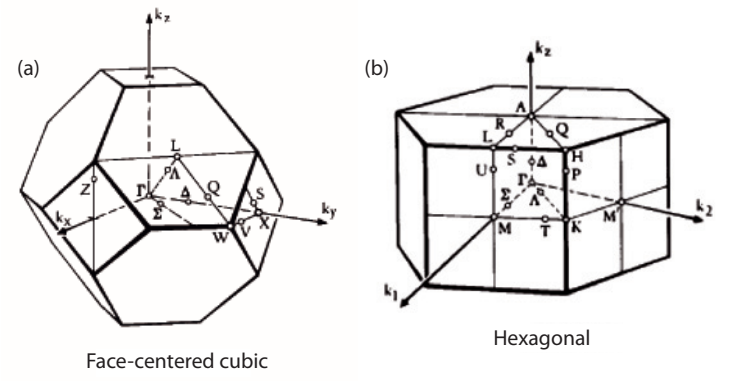

Figure 2.1: The high symmetry points and directions in the Brillouin zone for (a) face-centered cubic and (b) hexagonal lattice. *Copied from Ref. [55].*

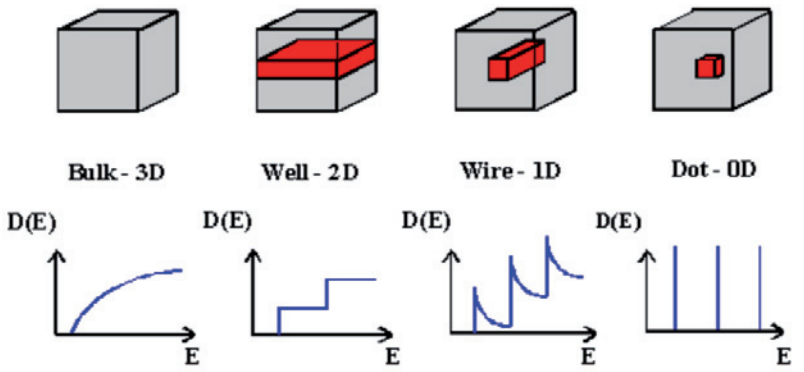

Figure 2.2: Schematics of bulk, two, one and zero dimensional structures and their associated density of states with respect to energy. *Copied from Ref. [56].*

For 0D (dot), the electrons are confined in the real space and their energy is constant in the **k**-space. In fact, the density of states of 0D structures is described as a set of delta functions. The electron densities of the 3D–0D structures as a function of energy are schematically illustrated in Fig. 2.2.

Beside the valence band, the core levels of a surface provide complementary information about the surface electronic structure. The core levels are the fingerprints for every element in the periodic table. Theoretically, the core level binding energy of a surface can be expressed as the total energy difference between the final state, i.e. the core hole system with $(N-1)$ electrons and the initial state with N electrons. Therefore, the core levels are very sensitive to physical and chemical surrounding of the surface. As a result, the presence of the slightest electronic perturbation such as surface restructuring and adsorbates can be detected in the core level PE spectrum in terms of binding energy shifts, as well as variation of the shape and intensity of individual peaks. The major synchrotron-based

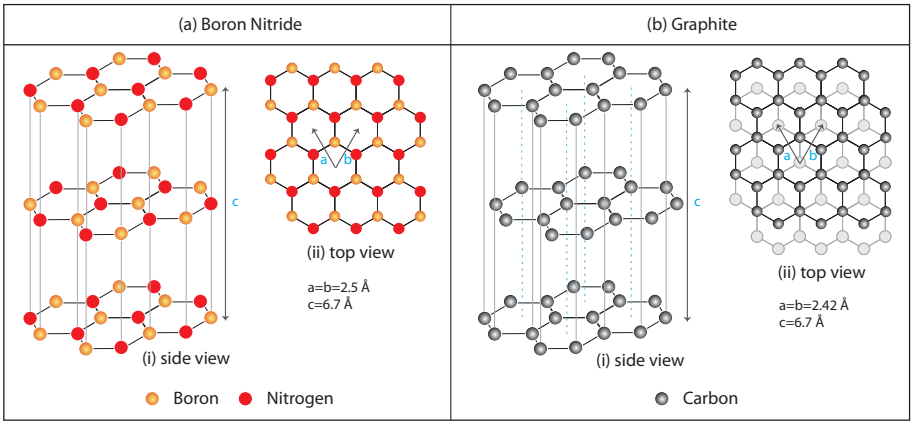

Figure 2.3: Molecular models for (a) boron nitride and (b) graphite, as viewed from (i) the side and (ii) the top.

experimental techniques specializing in surface electronic studies are photoemission spectroscopy (PES), x-ray absorption spectroscopy (XAS) and x-ray emission spectroscopy (XES). These surface characterization techniques are elaborated in Chap. 4.

2.1 Layered Materials

Layered or planar materials are extensively studied using the band theory since the early 40's. [57] Two well-studied classical examples are hexagonal boron nitride and graphite. In fact, the first calculation of the graphite electronic band structure was performed by Wallace [58] using the tight-binding approximation (TBA) in 1947. [59] These layered material consist of 2D sheets with strong bonds within the plane, which can be stacked on top of each other by the inter-planar interactions, as illustrated in Fig. 2.3.

2.1.1 Boron Nitride

Hexagonal boron nitride is an example of the wide-gap III-V compound semiconductor. It has a crystal lattice with $a = b = 2.5$ Å and $c = 6.7$ Å [60, 61]. Each crystal plane consists of anisotropic hexagonal structures consisting of B and N atoms, where B and N take alternate positions in the hexagon. The BN planes are commonly known to stack in registry with each other in such a way that the B and N atoms eclipse (the B atom is exactly on top of the N atom), owing to the electrostatic interaction between the B and N atoms (see Fig. 2.3(a)). However, this stacking is not the only stable stacking for h-BN, according to Ooi *et al.* [61]. Other studied stackings have similar stability and cohesive energy despite the different symmetries. Both bulk and single sheet h-BN have similar band gap close to 6.0 eV. The band dispersion diagrams for bulk and monolayer h-BN are also qualita-

tively quite similar (see Fig. 2.4). Both theoretical works [60, 61] report that h-BN is an indirect gap semiconductor, i.e. the lowest CB does not coincide with the highest VB at the same point of the BZ. Meanwhile, the lowest valence band is dominated by the N 2*s* orbitals, as depicted in Fig. 2.4.

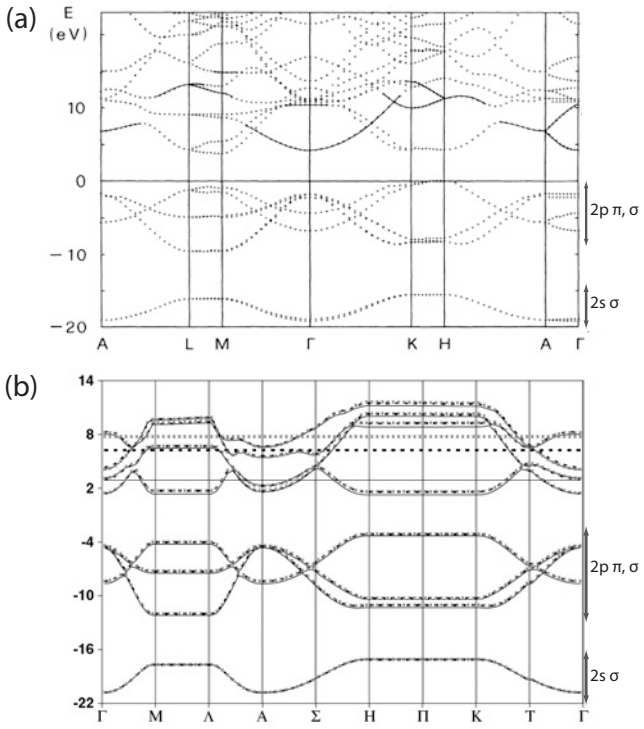

Figure 2.4: The energy band structures of (a) bulk and (b) single plane hexagonal boron nitride in the Brillouin zones. *Extracted from Ref. [61] respective Ref. [60].*

The total electron density is localized predominantly on the N-atoms because nitrogen is more electronegative than boron, as portrayed in Fig. 2.5. Both the basal plane and the inter-plane are consisting of B-N bonds. The basal ones are mainly strong covalent bonds with weak ionic character owing to the partial electron transfer from boron to nitrogen. This causes a large band gap between the occupied and empty states and forces the 2*s* σ-band to separate from the $2p$ π-bands, as shown by both band diagrams in Fig. 2.4. On the other hand, the interlayer orbital mixing is so small that the resultant interlayer chemical bond is practically non-existent. The only forces that keep the planes together are the weak quadrupole or higher order electrostatic interactions or polarization effects (van der Waals). [60] Hence, the electronic structure of bulk h-BN is prevailingly 2D (quasi 2D).

2.1.2 Graphite

Graphite has exactly the same hexagonal structure as h-BN although graphite consists solely of carbon atoms. In contrast to h-BN, graphite is

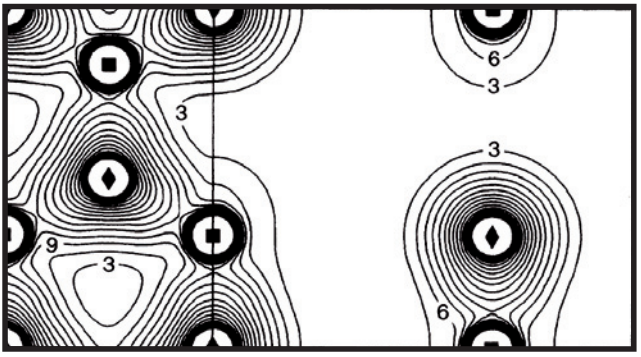

Figure 2.5: The total electronic charge density of hexagonal boron nitride basal plane [left] and vertical plane through a B-N bond [right]. Diamond represents nitrogen and square symbolizes boron. The contour value is 0.1 eÅ^{-3} and the contour difference is 0.3 eÅ^{-3}. *Extracted from Ref. [60].*

a gapless semiconductor and the successive graphite planes are shifted laterally from each other resulting in the Bernal stacking, as illustrated by Fig. 2.3(b). Unlike h-BN, this is the only stable stacking for graphite. The intra-planar C-atoms bond covalently (short bond length, 1.4 Å) while the adjacent inter-planes are bonded with weak van der Waals bond (long bond distance, 3.4 Å). Due to the weak inter-planar interaction, each plane can be considered as nearly isolated sets of C atoms in the electronic structure discussion. In the basal plane, each C has four valence electrons with three electrons forming sp^2 covalent bonds with the in-plane neighboring C-atoms and the forth electron forms π bond perpendicular to the plane, i.e. the p_z orbital. Since there is no distinction between the adjacent π bonds, the π electrons are delocalized and they form delocalized orbital clouds above and below the plane, namely the π conjugated system. These π electrons can travel freely within the plane with very little scattering, which are responsible for the excellent electrical conductivity in graphene.

The electronic structure of an isolated monolayer of graphene (MG) exhibits fascinating properties [45, 63] not found in the bulk. The key feature of the graphene electronic structure is the linear dispersion and the contacting conduction and valence bands at the **K**-points in the Brillouin zone resulting in a Dirac-like metallic Fermi surface [64], as shown in Fig. 2.7. Ballistic electron mobility in MG is observed due to the absence of electron backscattering and therefore the unhindered electron transfer above and below the 2D MG plane. Furthermore, point disorder is almost nonexistent in MG. These properties result in the high electron mobility of 200 000 cm^2/Vs at RT for free-standing MG and up to 120 000 cm^2/Vs at 240 K for suspended MG. [63]

Since MG has no intrinsic band gap that is crucial for many electronic technologies, it is apparent that band gap engineering is a necessity to enhance the versatility of MG. In fact, graphene inherits the possibility

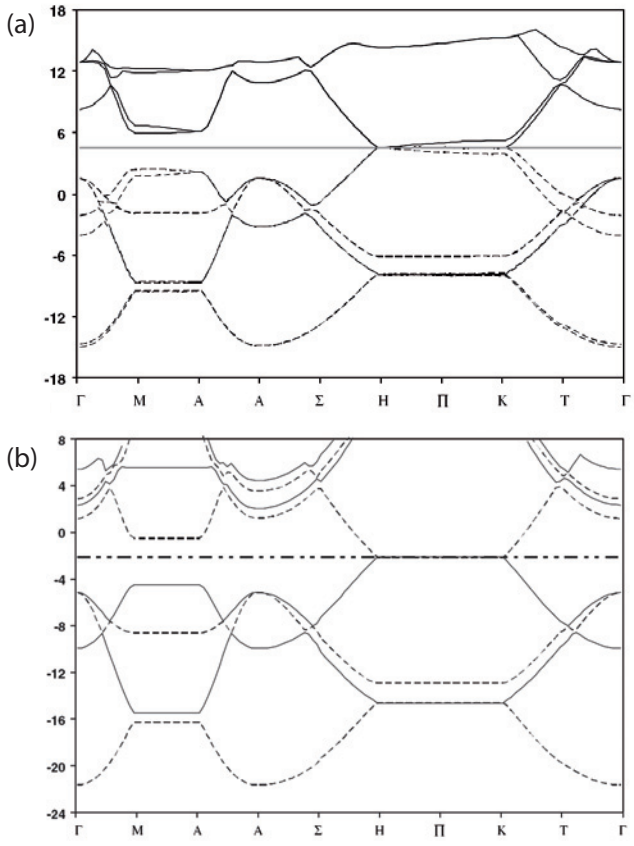

Figure 2.6: The energy band structures of (a) graphite and (b) graphene in the Brillouin zones. *Extracted from Ref. [62].*

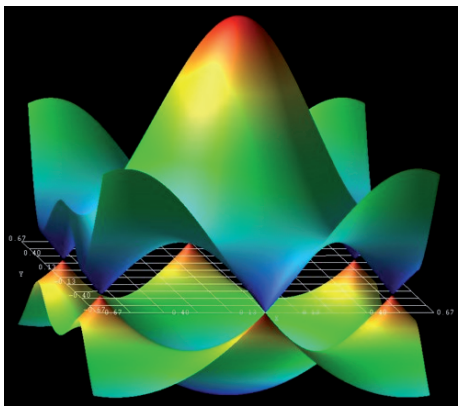

Figure 2.7: Tight-binding band structure of graphene π (bottom) and π^* (top) bands with Dirac-like distributions and touching at the **K**-points. *Copied from Ref. [65].*

for band gap modification, i.e by the quantum confinement of charges in graphene nanoribbons (GNRs). The atomic structure of GNR with homogeneously zigzag and armchair edges have astonishingly different π band properties, as forecasted by calculations performed in Ref. [66]. Theoretical predictions also show that GNR with perfect zigzag edge exhibits ferromagnetic metallic states while the armchair edges has a gap of a few hundred meV. [67] Atom and molecule adsorption on graphene is an alternative method to derive a band gap chemically. Many theoretical works have proven this possibility. For example, Ohta *et al.* [64] studied the gap evolution by potassium doping a bilayer graphene. They have shown that the gap opening can be controlled by the level of alkali atom doping. Ribeiro and co-workers [68] have shown that the adhesion of molecules, i.e. water and ammonia can induce a gap opening and displacement in monolayer as well as bilayer graphene. In addition, the gap value may also be dependent on the molecule orientation, adsorption site and coverage.

2.2 Transition Metals

According to the International Union of Pure and Applied Chemistry (IUPAC), transition metals are defined as d-block metals with partially filled d-states, or which can give rise to cations with an incomplete d-shell. Therefore all elements from group 3 to group 11 of the periodic table are classified as TMs. In TMs, the d-electrons are valence electrons often engaged in chemical reactions. The $(n+1)s$ orbital has the same or lower energy than the nd orbital. According to Watson *et al.* [69], the $3d$ electron orbital is much more compact than the $4s$ orbital and the nucleus–core electron Coulomb interaction for the $3d$-orbital is approximately twice that of the $4s$-orbital.

Due to the disparity in chemical nature and coordination between the surface and bulk atoms of a metal, the surface atom cohesive energy is not the same as for the bulk atoms. Consequently, there is a shift of binding energy, E_B for the core electrons in the surface atoms, from those in the bulk atoms, namely the surface core level shift (SCLS) [70, 71, 72, 73]. SCLS (ΔE_s) can be expressed as the following.

$$\Delta E_s = E_B(surf) - E_B(bulk) \tag{2.1}$$

where $E_B(surf)$ and $E_B(bulk)$ are the binding energy of the surface respective the bulk core electrons. For a metal with atomic number Z, the SCLS can be derived from the energy difference between the core initial and core-hole final states using the Born-Haber cycle that treats the initial state as a Z metal and the final state as a *(Z+1)* impurity dissolved in the Z metal. The binding energies of the bulk and surface core level electrons in a metal are

given below.

$$E_B(bulk) = A + E_{c,bulk}(Z) - E_{c,bulk}(Z+1) \quad (2.2)$$

$$E_B(surf) = A + E_{c,surf}(Z) - E_{c,surf}(Z+1) \quad (2.3)$$

where E_c is the cohesive energy and A contains all Born-Haber cycle terms that are not related to the environment of the core ionized atom. According to the detailed derivation of the *(Z+1)* approximation given by Johansson and Mårtensson [71], the SCLS of a metal with Z atomic number can be represented by the following:

$$\Delta E_s = (1-\alpha)[E_c(Z+1) - E_c(Z)] \quad (2.4)$$

where α is a value depending on the packing of the surface. This equation infers that the final state valence electron distribution around the core hole is an analogy to the *(Z+1)* element. The final states of the later TMs are screened by the anti-bonding part of the d-band and therefore, the initial states gain more in bonding energy than the final states. This explains the SCLS to the lower binding energy, i.e. negative SCLS. Although many TMs have negative SCLS, there are some with positive SCLS. For example, Re $4f$ and Os $4f$ have positive SCLSs, as published in Ref. [74] and Ref. [75], respectively.

Generally, the SCLS values for TMs evolve from positive to negative across the periodic table (from left to right). However, this general SCLS trend is not linear across the TM groups because of the slightly varied s-orbital occupation, e.g. monovalent ($d^{n+1}s^1$) and divalent ($d^n s^2$). An example for this deviation is the transition from Ir to Pt. This is because the screening by the delocalized s-electron of valence-nature on the the d-electrons has a significant impact on the final-state relaxation energy [76]. Beside final-state effect, SCLS is also influenced by the surface structural (crystal lattice, defects and reconstruction) as well as chemical (interaction and adsorption) properties. For example, van der Veen and co-worker [77] have shown that the SCLS in Ir is structurally dependent, i.e. it depends on the specific faces and their recontructions. The Ir $4f$ SCLS is 0.49 eV for Ir(100)-(5×1), 0.50 eV for Ir(111) and 0.68 eV for Ir(100)-(1×1).

2.3 Impact of Adsorption on the Electronic Structure

The work function of a surface system changes when adsorbates with unsaturated π bonds, such as -B=N- in h-BN and -C=C- in MG, interact with the metal surface dipoles, which causes electron donation from the highest occupied π-orbitals to the metal and back donation from the metal d-states to the lowest unoccupied π^*-orbitals. This is called adsorption induced charge transfer at the interface. [78] The measurement of work function of a surface system can therefore shed light on the charge transfer and consequently, on the details of the interfacial interaction.

For the h-BN case, Laskowski *et al.* [79] have calculated the impact of h-BN adsorption on Ru, Rh and Pt on the electronic structure. They have shown that there is a rigid shift of the core and valence states depending on the distance between the h-BN layer and the substrate. This shift is attributed to the non-uniform charge transfer from the h-BN layer to the metal. Consequently, there is a non-uniform electrostatic field above the overlayer, which simultaneously alters the surface space charge and thus the work function.

The first-principles study in Ref. [45] shows that the bonding of MG to Al, Ag, Cu, Au and Pt is weak, i.e. physisorption. Nevertheless, the charge transfer shifts the MG Fermi level by up to 0.5 eV with respect to the conical points. On the other hand, chemisorption of MG on Co, Ni, Pd and Ti reduces the work function significantly due to the $p_z - d$ states hybridization that opens a band gap in MG.

Upon interfacial reaction, the valence bands are re-hybridized. Thereby, changes in the valence and conduction bands after adsorption signify interaction activity and the degree of changes in the VB PE and NEXAFS spectra correlates with the strength of interaction. In solid adsorbates, the dispersion in the band structure may also yield information about the dimensionality of the adsorbed structures. As mentioned earlier, the band structure is non-dispersive for the 0D structures owing to the electron confinement in a quantum dot. Therefore, a non-dispersive metal band structure may be characteristic for an array of small particles with a narrow size distribution.

Most importantly, the modifications in the core level PE spectra of the adsorbate upon adsorption is the direct implication of an interfacial interaction. As a matter of fact, by analyzing the spectral profile of the core level, it is possible to detect the smallest variation in the surface chemical surroundings, to predict the strength of interaction and to estimate the amount of adsorbates.

The core level shift (CLS) [70] of the localized core shell of an adsorbate, e.g. B 1s, N 1s and C 1s, is a concept commonly used for studying the strength and type of adsorption, i.e. the chemical shift. This is because adsorption induces orbital hybridization, which can shift the unoccupied states with respect to the Fermi level. In chemisorption, the partial electron occupation of the π^* orbitals upon hybridization with the substrate results in a metallic screening of the adsorbate ionized core, i.e. the final-state effect. This causes a difference in the adsorbate final state before and after adsorption which in turn causes a CLS. For physisorption, the orbital overlap is almost insignificant. Here, the weak screening is accounted by the image potential from the polarized charge in the substrate.

Similar to the adsorbate-induced CLS, adsorption can also induce the SCLS of the substrate, i.e. adsorbate-induced SCLS. In a way, adsorption increases the surface coordination to the metal surface atoms. Typically, surface atoms gain energy upon chemisorption and thus, the surface component of the core level is shifted towards the higher binding energy. The adsorbate-induced SCLS for the TM 3d- and 4f-shell has been observed

in many experimental works. For example, the SCLS of Ru $3d$ and Rh $3d$ to higher binding energy due to the adsorption of oxygen on the metal surface. [80, 81, 82] SCLS in Pt $4f$ resulted from the adsorption of H, atomic and molecular oxygen and CO on Pt(110) [83] and the adsorption of molecular oxygen on Pt(111) [84], SCLS in Ir $4f$ due to oxygen adsorption on Ir(111) [85] and many others.

3. A Brief Research Review

3.1 Hexagonal Boron Nitride on TM Surfaces

There is a variety of BN deposition methods, e.g. thermal decomposition of and chemical reaction between B- and N-containing chemicals on both inert as well as reactive metal surfaces. Basche and Schiff (1964) [86] and Pierson (1975) [87] are two examples of the first studies on the pyrolytic deposition of boron nitride but the process consists of complicated chemical reactions and the product is way above a single layer of h-BN.

Paffett *et al.* (1990) [5] was one of pioneers in producing a single layer of h-BN by the adsorption of thermally decomposed molecular precursor, i.e. borazine ($B_3N_3H_6$), on single crystal TM surfaces, i.e. Pt(111) and Ru(0001). Borazine is a cyclic analog of benzene, where the C atoms are substituted with alternate B and N atoms and it has a natural 1 : 1 B-N stoichiometry for growing BN overlayers. Therefore, a chemical interaction between two or more gases, e.g. NH_3 + BF_3 [87] and NH_3 + B_2H_6 [88], is not necessary. Paffett and co-workers proposed that borazine was dehydrogenated completely at 1000 K and the morphology of h-BN monolayer formed on Pt were different from those on Ru. They suspected the difference in the interfacial bonding was responsible for the morphological change.

In 2004, Corso *et al.* [8] discovered a highly periodic corrugated structure of h-BN layer on Rh(111), which they originally interpreted as a double-layer mesh structure. The system is known as the h-BN nanomesh. Later, it was confirmed that the nanomesh structure originates from a single monolayer [17, 89]. It is a (13 × 13) h-BN superstructure forms on a (12 × 12) Rh substrate. [90] The B and N atoms have two types of chemical state, i.e. "holes" (bonding part) and "wires" (non-bonding part) of the nanomesh. [91] A micrograph of the nanomesh structure is shown in Fig. 3.1.

This nanomesh model is further confirmed by *ab initio* force field calculations in Ref. [89] and full/direct *ab initio* calculations with density functional theory (DFT) in Ref. [91]. Furthermore, the latter calculations are also capable of predicting the STM images of the nanomesh, which agree well with experimental STM measurements. The h-BN nanomesh forms strictly on only two TMs, namely Rh(111) and Ru(0001) because these substrates have similar lattice constant and surface reactivity, which are the important factors for achieving the overlayer corrugation [92]. Many works have proven the prospect of using the h-BN nanomesh as a template. [93, 94, 95]

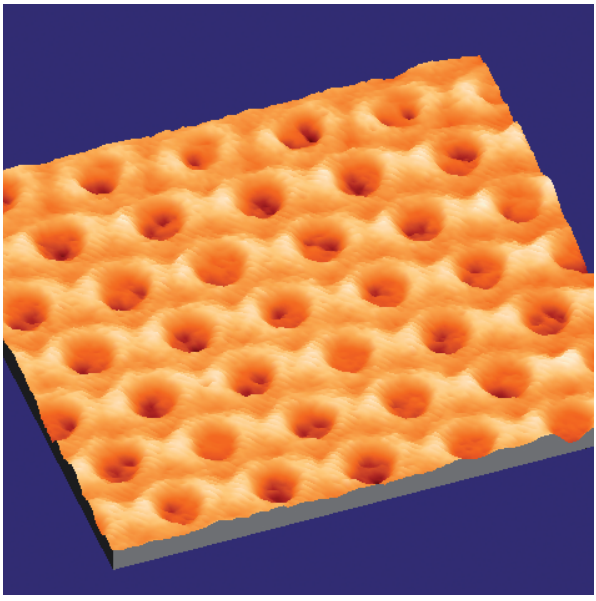

Figure 3.1: A STM image of the 17 × 17 nm BN nanomesh showing the "holes" (bonding part) and "wires" (non-bonding part).

The strongly interacting h-BN on Ni(111) system is one of the best studied h-BN/TM systems. [6, 7, 9, 44, 96] It is well-known that the interfacial interaction of this system is strong and that the perturbation of the electronic structure is visible in the valence band. This interface is lattice matched, i.e. it results in a commensurate overlayer with an (1 × 1) LEED pattern. There are other h-BN/TM systems that are lattice mismatched such as h-BN/Pd(111) [6, 97] and h-BN/Pt(111) [6, 98], which result in a Moiré pattern between the overlayer and the substrate.

3.2 Monolayer Graphite on TM Surfaces

More than 70 years ago, Landau and Peierls stated that graphene could not exist in reality because such a thin film was thermodynamically unstable. [12] Naturally, the next option is to put graphene on a substrate. But, the experimental search for MG on TMs started relatively recently, i.e. in the early 1970s. As a matter of fact, the first results of multilayer graphite grown by chemical vapor deposition (CVD) on various substrates were both published in 1966 by two separate groups [99, 100], according to Oshima and Nagashima in Ref. [2]. In CVD, hydrocarbon gases are used as molecular precursors. Unsaturated hydrocarbons (C_nH_{2n}, n> 1) such as ethene and propene are preferred over the saturated (C_nH_{2n+2}) ones because they contain less H-atoms and therefore, more readily to be fully dehydrogenated. The C-H bonds are cracked upon adsorption on a heated (ca. 1000 K) TM surface, eliminating the H-atoms as H_2 molecules by desorption from the

surface and the remaining carbidic molecules "find each other" and form a graphene layer on the TM surface. In the 70s and 80s, an alternative method for growing MG was also used, i.e. by C-atom segregation [2] from C-rich transition metal carbide (TMC) substrates (e.g. SiC, TiC and TaC) to the surface by annealing the substrate to a very high temperature.

These studies were mainly devoted to prove the possibility to grow monolayers of graphene and fine tuning of the growth methods by varying the preparation parameters, e.g. substrate temperature that determines the rate and efficiency of precursor cracking and that together with the precursor flux controls the rate of adsorption. A majority of these graphitic overlayers were probed by LEED, which in principle only gives local qualitative structural information, i.e. the orientation of the overlayer with regard to the substrate and the information is only valid for the electron gun impinging area. [101] Other characterization methods were angle-resolved ultraviolet photoelectron spectroscopy (ARUPS), high-resolution electron energy-loss spectroscopy (HREELS) and ultraviolet photoelectron spectroscopy (UPS). With only modest technical resources, experiments and theoretical calculations were limited to rather simple systems and the data collection process was hindered severely by technical limitations such as poor resolution.

From the late 80s onwards, in parallel with the booming of synchrotron light sources and rapid progress in technical and computing equipments such as scanning tunneling microscopy (STM) and computers, advanced and complicated experiments could be performed much easier and faster and more detailed insight and understanding on the graphitic systems were gained. In 1995, Nagashima [102] studied the MG growth rates and he stated that the growth rate of MG is reduced 1/10 – 1/100 by the first MG. Since the dehydrogenation rate on the TM surface is reduced drastically by the first complete MG, it is possible to have precise control on the thickness of the MG grown.

There are many proofs of the varying strength of interaction between MG and TM or TMC surfaces. The deferred band structure and work function after the adsorption of MG on these surfaces are obvious evidences that MG interacts with the TM (TMC). Oshima and Nagashima [2] compared the normal MG on an inert TiC(100) surface and the soft MG on a reactive TaC(111) surface and identified profound differences in the electronic structures. On TiC(100), the MG electronic structure is similar to that of bulk graphite. On TaC(111), the binding energy of the MG π-band is shifted downwards relative to the π-band of bulk graphite. Instead of the π-band touching the Fermi level at the **K**-points, it has a band gap of about 1.3 eV. In addition, work function measurements have shown a common decrease in work function upon deposition of MG and the decrement is proportional to the interfacial interaction. The lowering of the work function due to the interaction between MG and the substrate is explained by the asymmetric charge distribution on the graphitic layer, i.e. the charge distribution along the interface is different from that on the vacuum side. This asymmetry in-

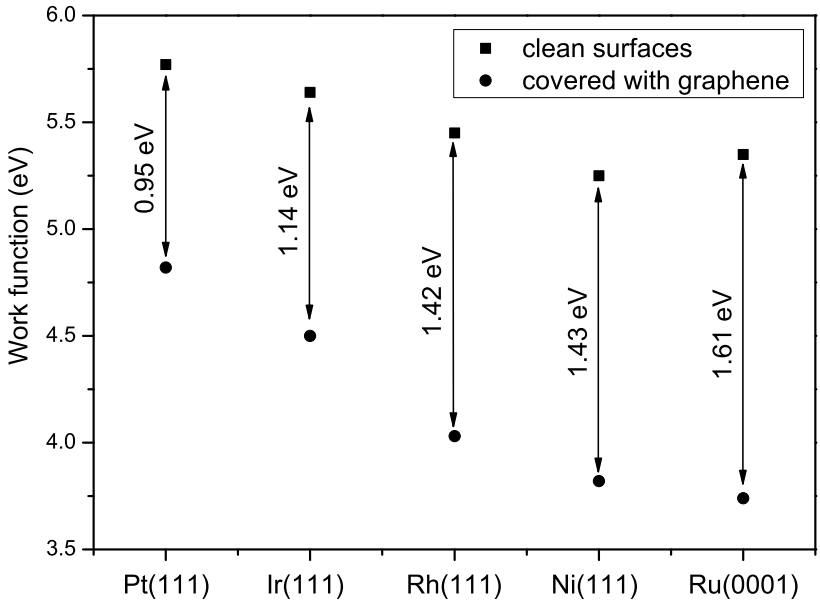

Figure 3.2: A summary of the work functions of the Pt, Ir, Rh, Ni and Ru surfaces before and after the adsorption of graphene. *Unpublished work.*

duces an electric dipole perpendicular to the surface and hence a reduction of the work function. Fig. 3.2 shows the shift in work function upon adsorption of MG on various TMs.

The decreasing interlayer spacing between MG and the topmost TM with increasing interaction strength as compared to the interplanar distance (in graphite) is another sign of interaction. The weak van der Waals interplanar bond length is about 3.4 Å while the strong MG/Ni(111) bond length is 2.1 Å [103]. Gall and co-workers [14, 43] studied the nature of bonds between 2D graphite films and metals. Here, they gave a detailed account to modes and mechanisms of intercalation of various atoms and molecules through the MG layer. They attributed the intercalation/penetration efficiency to mainly two factors, i.e the ionization potential of the penetrating atom and the strength of MG–TM interfacial interaction. Furthermore, intercalated metals can also be used to largely eliminate the MG–TM or MG–TMC interaction resulting in an almost free standing MG layer. The bond softening by intercalation of Cu on the strongly interacting MG/Ni(111) is observed by Shikin *et al.* in [104]. This can also be observed in the MG/TMC system, i.e. the disappearance of the 3D π states of MG/SiC upon the intercalation of K or Rb, whereby the band structure becomes more graphene-like. [105]

For single crystal metals that are lattice mismatched with MG, there is a correlation between the degree of mismatch and the surface corrugation, similar to the BN nanomesh. The resulting corrugated surface with uniform physical barriers can be used as a template for decoration with atoms and molecules. For example, N'Diaye and co-workers [106] observed that

MG/Ir(111) formed a Moiré pattern and decorated the MG template with Ir adatoms. Subsequently, they observed a monodispersed, hexagonal Ir cluster array on MG. As the coverage of Ir approached 2 ML, the clusters developed into triangular structures. This is an important discovery toward functionalization of the immaculate graphene layer for catalytic studies.

Recently, Moritz *et al.* performed detailed LEED I(V) studies and DFT calculations for the MG/Ru(0001) system. They have suggested that the surface of the (25 × 25) MG overlayer on the (23 × 23) Ru substrate is corrugated. The corrugation is similar to the inversed h-BN/Ru nanomesh, i.e. the bonding parts become non-bonding and *vice versa*. [107] This model agrees with the one published in Ref. [108]. In contrast, the surface x-ray diffraction (SXRD) results by Martoccia *et al.* suggest that the corrugated MG/Ru overlayer forms a triangular mesh, i.e. triangular islands of non-bonding graphene alternating with bonding areas. [109, 110]

For the lattice matched cases, namely the strongly interacting Ni and the weakly interacting Cu, surface corrugation is not possible. For MG/Ni, it is shown by LEED studies that one carbon atom adsorbs on top of a Ni atom and the adjacent carbon atom in the fcc hollow site. [11, 103] The MG adsorption on Cu was only predicted theoretically [11, 111, 112] until very recently that MG/Cu was successfully produced. First, it was grown on a polycrystalline Cu foil [113] and then on a single crystal Cu(111) surface [114].

4. Surface Characterization Techniques

4.1 Photoelectron Spectroscopy

Photoelectron spectroscopy (PES) is an indispensable tool for surface studies because of its high and tunable surface sensitivity. By varying the incident photon energy or angle, PES can be tuned to excite electrons from predominantly the surface atoms or such atoms with influence from the interface. This allows the study of the overlayer as well as the interface between the overlayer and substrate. In addition, PES is element specific since all core level electron binding energies are unique and hence constitute fingerprints for each element. Therefore, PE techniques have been utilized extensively in this work to study the morphology and chemical bonding of adsorbed overlayers.

4.1.1 The Principles of PES

The entire idea of PES is rooted from Einstein's phenomenal discovery of photoelectric effect, which can be explained by Eq. 4.1.

$$h\nu - \phi = E_k \tag{4.1}$$

where $h\nu$ is the photon energy, ϕ is the material work function and E_k is the photoelectron kinetic energy. Owing to the fact that electron binding energy, E_B is very unique to each quantum level of each species, it is used to identify all elements in the periodic table.

$$E_B = h\nu - \phi - E_k \tag{4.2}$$

For the known photon energy and work function, E_B can be determined by measuring the photoelectron kinetic energy. Despite the simplicity of this equation, the experimental PE spectrum represents a statistical distribution due to the finite life time of the core-excited state, final-state effects, experimental broadening, etc. Thus it is inevitable to include these factors in the theory of PES in order to ascertain accurate interpretation of the data.

For the ideal 1-electron system, i.e. hydrogen atom with only one core level populated by only one electron, it is straight-forward to promote the electron to the continuum as a photoelectron with the kinetic energy equals to the photon energy, $h\nu$ less the H $1s$ Koopman binding energy, E_B (because there is no options for electron relaxation). The final state of the ion-

ized H has an infinite hole lifetime and therefore, the H 1s spectrum has a pure Gaussian distribution owing to broadening in the measurement.

In reality, the studied object has certainly more than one electron and these electrons can correlate with each other under the constitution of Pauli exclusion principle. Therefore, the final state of the core-ionized system is profoundly modified due to the interaction between the core hole and the remaining system. The finite probability of the decay processes result in the finite core hole lifetime, which is characterized by the natural (Lorentzian) broadening of the photoelectron lines.

In general, the photoemission process can be divided into three steps, hence the name 3-step model, as proposed by Berglund and Spicer [115]. Although this model is less accurate than the 1-step model, it is nonetheless more instructive. The steps are as listed below.

1. photoexcitation of an electron in a solid
2. propagation of the photoelectron to the surface
3. escape of the electron from the surface to the vacuum

For photoionization of core electrons with photon energy of $h\nu$, the transition probability obeys the Fermi's Golden Rule, as given in the following.

$$w_{fi} = \frac{2\pi}{\hbar}|\langle \Psi_f, \mathbf{K}_f | H^{int} | \Psi_i, \mathbf{k}_i \rangle|^2 \delta(E_f - E_i - h\nu) \tag{4.3}$$

where E_i is the energy of the multielectron system in the initial state i with the wave function ψ_i and E_f is the energy of the system in the final state f with the wave function ψ_f. The Hamiltonian for the interaction between an electron and the photon electromagnetic field is represented by

$$H^{int} = \frac{e}{mc}\mathbf{A}\cdot\mathbf{p} \tag{4.4}$$

where $\mathbf{A}$ is the vector potential of the photon electromagnetic field and $\mathbf{p}$ is the momentum operator of the electron. Due to conservation of the wave vector parallel to the surface, $\mathbf{K}_f = \mathbf{k}_i + \mathbf{G}$ where $\mathbf{G}$ is the 2D reciprocal lattice vector. For electric dipole approximation of the Hamiltonian, the transition is governed by the selection rules, namely the spin rule, $\triangle S = 0$ and the orbital rule, $\triangle l = \pm 1$.

When the excited electron propagates to the surface, it experiences energy losses due to the scattering and electron-electron interaction and thus the number of photoelectrons reaching the surface is reduced. The electron inelastic mean free path (IMFP), λ is the distance an electron travels without significant energy loss due to inelastic processes and the probability of the electron escaping is e^{-1} less than the original value. The universal curve for electron IMFP is shown in Fig. 4.1. IMFP is a function of the excitation energy, E and wave vector, k, as in Eq. 4.5.

$$\lambda(E,k) = \tau v_g = \frac{\tau}{\hbar}\frac{dE}{dk} \tag{4.5}$$

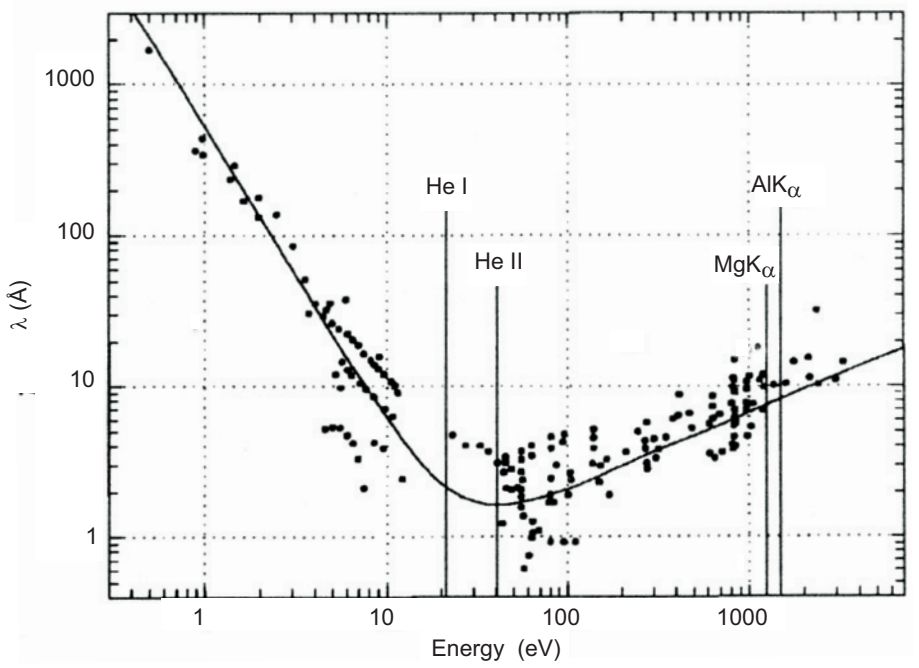

Figure 4.1: Photoelectron inelastic mean free paths, λ as a function of their kinetic energy for different elements. *Copied from Ref. [116].*

where τ is the scattering lifetime and v_g is the electron group velocity in the final state. At low energies ($20-30$ eV), electrons can propagate a long distance without much obstacles because scattering is weak. From 40 to 200 eV, scattering processes are most favorable due to the peaking scattering cross sections. Therefore the electron IMFP dips in this energy range. At higher energies, IMFP increases with energy due to the shrinking scattering cross section. Normally, the electron IMFP is short, i.e. between a few and a few tens of Å for soft x-ray energy range, which makes PES suitable for measuring electronic states in the surface region. However, due to the short IMFP, it is necessary to perform the measurement in UHV (10^{-9} mBar and below) to minimize photoelectron scattering on the way to the detector.

The propagation of photoelectron from the solid surface into the vacuum is analogous to light refraction at the interface of two media with different refraction indices, as illustrated in Fig. 4.2[1]. Hence, Snell's law is applicable to explain the escape of photoelectron from the solid into vacuum. As a consequence, the wavevector parallel to the surface is conserved, whereby $K_\parallel = p_\parallel/\hbar = k_\parallel + G_\parallel$ is the momentum relation at the solid-vacuum interface.

[1] $\mathbf{k}$ designates the wave vector of Bloch states in a crystal, $\mathbf{K}$ designates the wave vector of the photoexcited electrons within the crystal and $\mathbf{p}/\hbar$ designates the wave vector of the photoelectrons outside the crystal in the vacuum

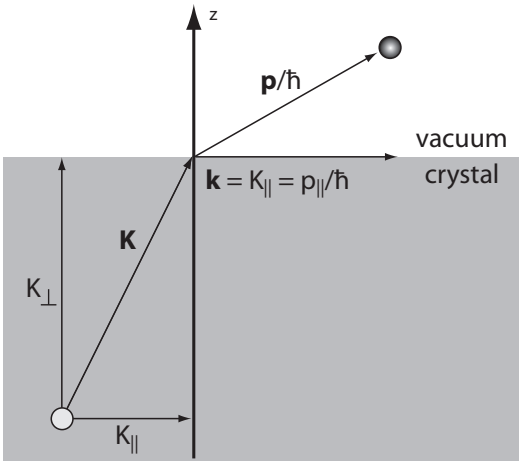

Figure 4.2: Electron momentum relations at the solid-vacuum interface.

Beside the direct photoemission processes (Fig. 4.3(a)), the PE spectrum is affected by secondary (de-excitation) processes. The descend of higher core electrons to fill the core holes causes the liberation of Auger electrons (Fig. 4.3(b)). The position of Auger electron peak in a PE spectrum is dependent on the photon energy but the core level peak has fixed binding energy. This fact is useful in differentiating the origin of the peaks in a spectrum, i.e. Auger peaks shift (on the binding energy scale) with the photon energy, while the photoelectron peaks are always fixed. For the sake of completeness, it should be mentioned here that the de-excitation by x-ray emission (Fig. 4.3(c)) is not contributing to the PE spectrum because it is a photon-out process.

Another process accompanying the primary electron transition is the occurrence of shake-up satellites (Fig. 4.3(d)) that may appear in the core-level spectrum at lower kinetic energies than the main lines. During the promotion of a core electron to the continuum, the core excitation can be accompanied by an additional excitation in the valence band. In the event that a valence electron is liberated from the system, the satellite associated to this process is called shake-off. In metals, it is a collective oscillation of the valence electrons relative to the positively charged core hole that can create intrinsic plasmon. Plasmons show up in the core level spectrum as asymmetric sidebands. Although it is often difficult to distinguish between intrinsic and extrinsic loss processes in solids, some interband transition with more localized character with strong influence from the core hole are significant. The notable example is the shake-up satellites of Ni 3d that appears at ca. 6 eV higher than the core level binding energy. [117, 118]

In the event of electron transitions from two almost coinciding core levels, e.g. of two or more different species, Cooper minima in the photoemission cross section of these core electrons can be utilized to reduce the probability of photoemission from one species while enhancing the contri-

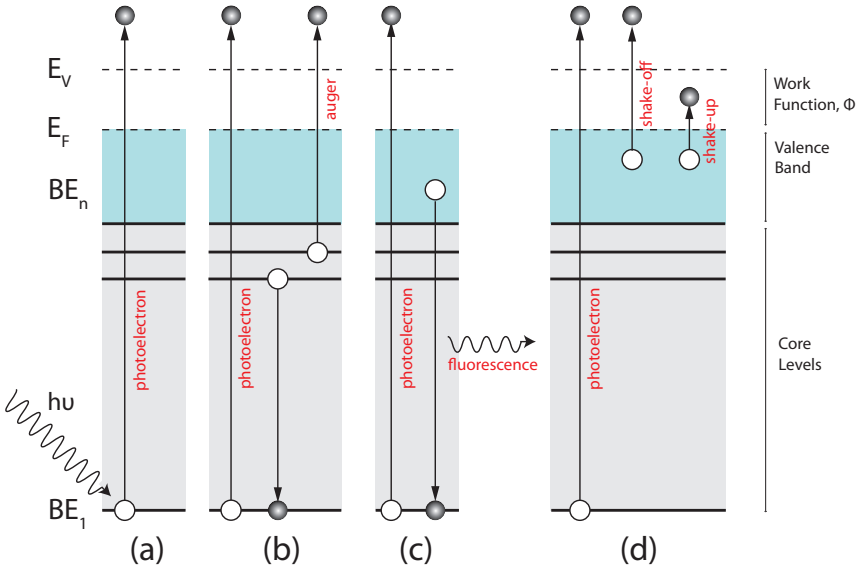

Figure 4.3: Schematics of PE processes in a solid. (a) Photoexcitation of a photoelectron into the vacuum resulting in a core hole. The ejection of a photoelectron can be accompanied by other de-excitation processes such as (b) the Auger process, (c) x-ray fluorescence and (d) multi-electron satellites.

bution from the other species. This is achieved by setting the photon energy to the specific Cooper minimum of the selected species.

4.1.2 Core Level PES

In core level PES, a core electron is liberated to the vacuum and its kinetic energy is measured. This is used extensively throughout this work because even small variations in the core level PE spectra are very informative for determining both physical and chemical properties of a surface [70].

Chemical shift (CS) is undoubtedly the most essential aspect of core level PES. CS can be defined as the difference between the energy of a photoelectron line for an element in a specific compound and the corresponding energy for the element in its pure state. Therefore, CS can be employed to distinguish and identify the specific species on a sample, the type of chemical bonding between the adsorbate and at the interface as well as the bond geometry. For example, CS is used to differentiate surface adsorbates from the bulk and top layer from the lower layer of e.g. a multilayer system, to identity the adsorption sites (top, bridge and hollow sites) and to reveal the degree of hybridization between adsorbate and substrate.

Each component of the PE core level spectrum represents a species with a particular chemical state. For example, Fig. 4.4(a)[thick blue curve] and [thick red curve] from Paper I show that the N 1*s* PE spectrum of h-BN monolayer adsorbed on Pt(111) measured with a surface sensitive (470 eV)

respective bulk sensitive (570 eV) photon energy, consist of predominantly a single component at 397.18 eV. This is because there is only one type of chemical environment for the N-atoms on Pt. In contrast, when h-BN is adsorbed on Rh, the N 1*s* spectra (Fig. 4.4(b)) show two distinctive components, i.e. N1 at 397.90 eV and N2 at 398.58 eV. These signals correspond to two types of the h-BN species on Rh, i.e. the non-bonding (wire) and the bonding (pore) h-BN.

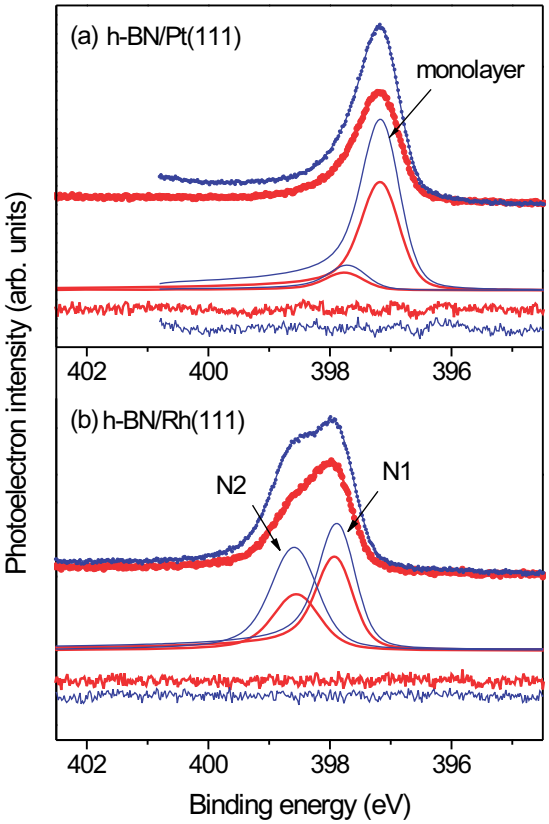

Figure 4.4: N 1*s* PES of (a) h-BN/Pt(111) showing a strong component and a small shoulder, and (b) h-BN/Rh(111) showing two prominent components, namely the non-bonding component, N1 and the bonding component, N2. The thick blue curves are recorded with photon energy 470 eV while the thick red curves with 570 eV. The thin blue and red curves represent their respective deconvoluted components of the thick curves. *From Paper I.*

The core level line shape is a convolution of a Lorentzian core-hole lifetime broadening and a Gaussian instrumental broadening, which causes the energy distribution to deviate from the ideal delta function. Asymmetry in the PE spectrum may occur due to the screening of the core hole, but this is more pronounced in metallic systems. Ref. [119] and Ref. [120] provide a detailed theoretical treatment of the line shape and the background of core level spectra from metals.

4.1.3 Valence Band PES

Since all chemical interactions involve the valence electrons, it is possible to probe the surface chemical composition and the interfacial bond strength by the valence band (VB) photoemission. In principle, the VB PE process can also be treated within the 3-step model as elaborated in Section 4.1.1, but it is only an approximation. In order to describe the process correctly, the true final state has to be taken into consideration and this can be achieved by applying the reversed low energy electron diffraction (LEED) wave function to the transition probability given in Eq. 4.3.

VB PES is performed by tuning the excitation photon energy so that the periodic lattice potential allows direct transitions into the reduced zone scheme, i.e. $h\nu < 100$ eV so that the photon momentum is negligible and the excited photoelectron momentum is normal to the surface. With this, the electron momentum parallel to the surface, $k_{||}$ is conserved. VB PES is used to study the impact of adsorption on the valence band of a surface.

Angular resolve photoelectron spectroscopy (ARPES) is a technique used for mapping the dispersion relations of the ion states of crystalline solids and well-ordered surfaces in the k-space. In principle, the concept of ARPES is similar to VB PES, i.e. the conservation of $k_{||}$. In ARPES, the PE intensity is measured as a function of the binding energy, E_B and the electron momentum parallel to the surface, $k_{||}$, which depends on the detection angle, θ, and kinetic energy, E_{kin}. The relation between these parameters is given in Eq. 4.6.

$$k_{||} = \sin\theta \sqrt{\frac{2m_e}{\hbar^2} E_{kin}} \tag{4.6}$$

where m_e is the electron mass, $\hbar$ is the Planck constant divided by 2π, $E_{kin} = h\nu - E_B - \phi$ with E_B the photoelectron binding energy and ϕ the surface work function.

In this thesis, ARPES is used to map the band structure of ordered overlayers adsorbed on TMs. This allows the study of the chemical state of a surface by analyzing the band shifts and the dispersion relation of individual bands.

4.1.4 Photoelectron Diffraction

Photoelectron diffraction (PED) is a structural technique that does not require long-range order on the surface structure. In general, there are two modes of PED measurements, namely, at fixed photon energy with varying photoelectron detection angle and at constant experimental geometry with varying photon energy. The first method measures the photoelectron intensity at gradually varying azimuthal or polar detection angle. The alternative method, which is the method used in this work, detects photoelectron intensity at a fixed angle while step-wise changing the incident photon energy. This is also known as the scanned-energy mode. In this thesis,

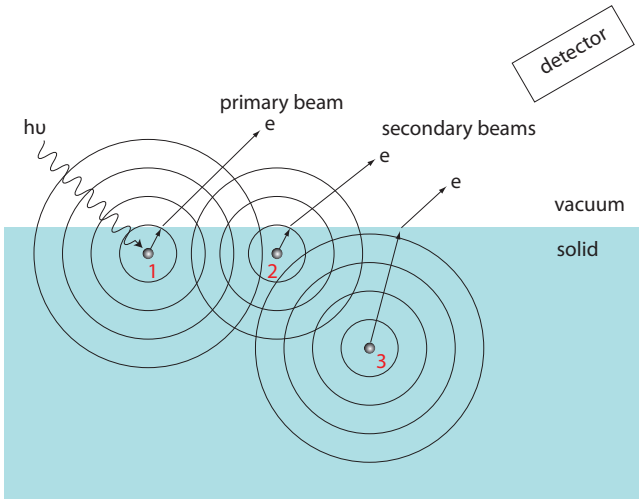

Figure 4.5: Scattering processes occur during PED. Photoexcitation of an electron results in a primary spherical wave that escape into the vacuum as primary beam (1). Inside the solid, the primary wave can be scattered by other ions (2) and (3) and escape the solid as secondary beams. *Diagram based on Ref. [122].*

the chemical-shift PED [121] is employed. The occurrence of bonding and non-bonding sites in the adsorbed h-BN and MG overlayers is due to two different chemical states of the same species on the sample. This results in a CS in the core level spectrum of the species. Therefore, CS PED in scanned-energy mode is used to determine the quantitative geometrical property of each chemical state.

When the photoelectron travels from the photoemission sites to the vacuum level, it will be scattered by the crystal lattice on the way out through the crystal. (see Fig. 4.5) The wave property of photoelectrons enables interference between the primary beam (spherical wave) from the emitter and secondary beams from the neighboring scatterers (or other ions in the crystal). And since electrons are also particles, they can be detected and counted as charges.

4.1.5 The Equipment

At Beamline D1011, MAX-lab, Lund University, the front chamber is facilitated with the Scienta SES 200 hemispherical electron analyzer. Fig. 4.6 depicts the technical drawing of a SES 200. The analyzer consists mainly of an electrostatic optics (entrance lens and hemispheres) for separating photoelectron trajectories and imaging them on the position sensitive multi channel plate (MCP) detector, a charge-coupled device (CCD) camera for capturing the electron counts and a computer-steered electronics and detection system. A detailed technical description of the spectrometer is available at the manufacturer's website. [123]

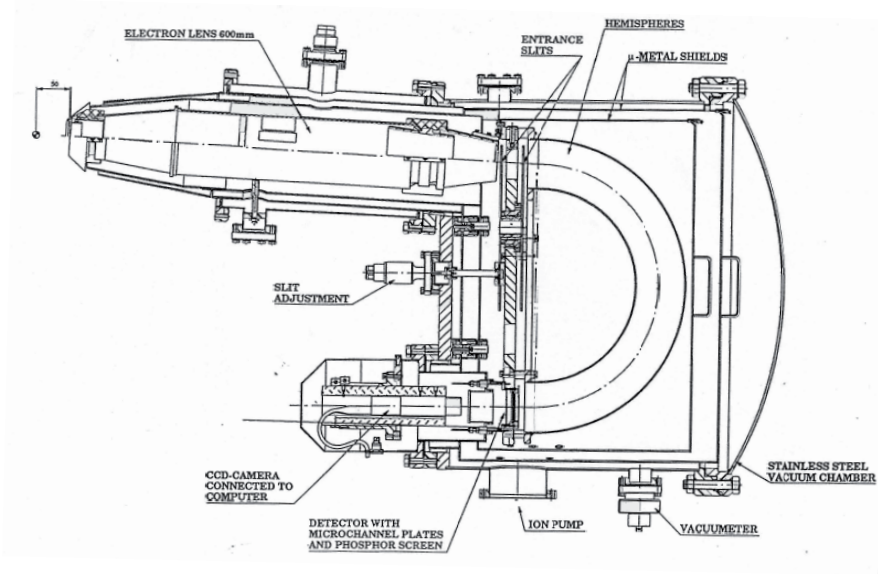

Figure 4.6: A technical drawing of Scienta SES-200 hemispherical electron analyzer

4.2 Near Edge X-ray Absorption Fine Structure

NEXAFS [124] is a powerful surface technique, which is both element and symmetry selective and very sensitive to the changes in the electronic structure of adsorbates induced by the substrates. The orientation of the molecules or functional groups on surfaces is highly responsive to the polarized synchrotron light, e.g. the π electrons of linear or plane molecules are strongly excited by grazing incident light (photon electromagnetic field parallel to the bond direction) if the molecules lie flat. For example, Fig. 4.7 shows the NEXAFS spectra at C K-edge of ca. 1 ML of pentacene on h-BN/Rh(111). From these spectra, it is evident that the pentacene molecules are standing up on the BN nanomesh because the π-resonances are responding weakly to the grazing incident photons but very strongly to the normal incident photons. For simple molecules, the exact tilting angle relative to the surface can be approximated by measuring a series of spectra at gradually changing photon incident angle and by performing an intensity analysis on these spectra.

Within the molecule, NEXAFS technique is sensitive to the structure of the nearest neighbors because intramolecular bonds are short bonds (1.1 – 1.5 Å), which give large backscattering amplitude and thus, prominent resonances up to 30 eV above the edge. These resonances are very sensitive to the chemical state of the probed atom. For example, the energy separation between the π- and σ-resonances in the spectra of linear and plane molecules is inversely proportional to the strength of chemical bonding. Meanwhile, shoulders and other fine structures appearing in the pre-edge region contain information not only on the chemical bonds

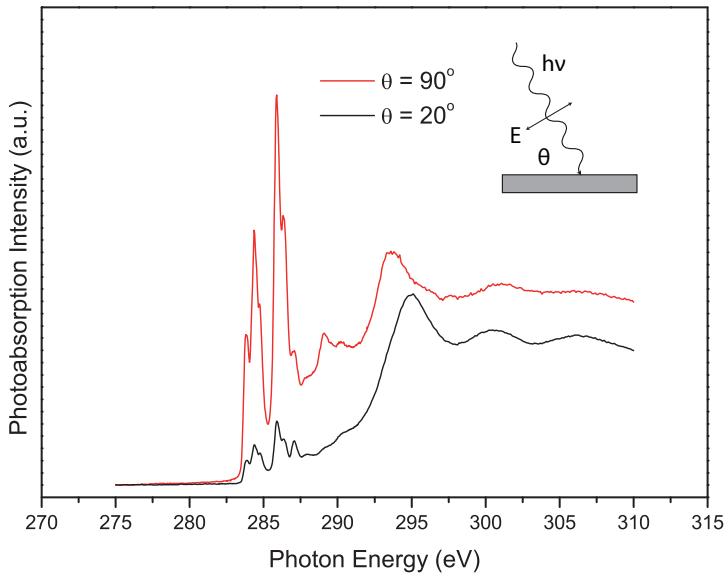

Figure 4.7: Angle dependent NEXAFS at C K-edge of ca. 1 ML of pentacene on h-BN/Rh(111) measured with photons at grazing (20°) and normal incident (90°) angle.

within the molecule or solid cluster but also on the adsorbate-substrate interaction.

In the process of x-ray absorption, the core electrons are excited to unoccupied valence states and this excitation triggers decay processes, i.e. fluorescence and Auger electron decay. The decay rate is proportional to the hole creation rate, i.e. the absorption coefficient. The intensity ratio between the Auger electron yield and fluorescence yield depends on the atomic number Z, i.e. it decreases with increasing Z. For NEXAFS, the number of electrons arriving at the detector with an energy of the characteristic $W_\alpha XY$ Auger line (W_α is the absorption edge of the element α, X is the relaxing electron initial state and Y is the emitted electron initial state), N is represented by Eq. 4.7.

$$N = N_{W_\alpha XY}(h\nu) + N_B(h\nu) \tag{4.7}$$

where $N_{W_\alpha XY}$ is the Auger count at the respective transition energy that can be converted to the absorption intensity and energy and N_B is the background signal. For detecting and counting of the Auger electrons, MCPs are employed at Beamline D1011. The detection modes are optional between total electron yield (TEY) and partial electron yield (PEY). For PEY, the slow electrons, which contribute to the background signal, are repulsed by applying a small negative voltage (e.g. -100 V) to a fine metal mesh positioned above the multi channel plates. Therefore, the PEY mode is a more surface sensitive than the TEY mode.

4.3 X-ray Emission Spectroscopy

X-ray Emission Spectroscopy (XES) can be divided into resonant and non-resonant (a.k.a normal) XE. Here, only non-resonant XES (NXES) is discussed and thus, the abbreviation XES means NXES.

In XES measurement, the incoming photon energy is set above the ionization energy of a core level in order to excite the core electron to the vacuum and simultaneously creating a core hole. When a valence electron fills the core hole, the transition energy is released in the form of emitted x-rays. The spectrum of these emitted photons is measured in XES. The initial state of XE is actually the final state of core-level PES, i.e. the ionized core state. The final state of XE is related to the final state in VB PES, i.e. the ionized valence state. The emission intensity for electron transition from the core ionized state to the valence ionized state is governed by the Fermi's golden rule as given in Eq. 4.3 and the transition obeys the dipole selection rules as stated earlier in section 4.1.1.

In this work, XES is utilized for probing the gap states of adsorbed overlayers. By combining the NEXAFS and XES results, the gap states of bulk h-BN and adsorbed h-BN/TMs can be compared. Since bulk h-BN is an insulator, there should be no gap states. However, upon adsorption on strongly interacting substrate, new gap states may appear due to orbital mixing.

4.4 Low Energy Electron Diffraction

LEED is a fast structural technique because it is simple to move the desired area of the sample into the electron beam and the diffraction patterns are produced instantaneously. It is ideal for determining the local structure of well-ordered overlayers both qualitatively, i.e. symmetry and rotational alignment of overlayer relative to the substrate and quantitatively, i.e. precise atomic positions, using I-V curve measurement (not used in this work and therefore not discussed here).

A LEED pattern shows the relation between the (1×1) substrate lattice and the overlayer superlattice, in terms of translational and rotational vectors in reciprocal space. By knowing the real space lattice parameters of the substrate, the parameters for the adsorbate can be calculated based on the LEED pattern.

In this work, LEED is used primarily to check the crystallographic quality of single crystal surfaces. The quality of an adsorbed overlayer can also be checked with LEED because contaminations and crystallographic imperfections can broaden spots and increase background to signal ratio, which would deteriorate the quality of the LEED patterns. The overlayer superstructure unit cell parameters can be determined from the LEED pattern if the unit cell parameters of the underlying substrate are known. Beside these, LEED reconstruction is also used as a guide to rotate the sample to the desired direction of the Brillouin zone for ARPES.

Beamline D1011 is equipped with a Omicron SPECTALEED optics at the front preparation chamber. The principle components of the optics are electron gun, grids and phosphor screen. Details of the LEED equipment and operation are available in Ref. [125].

4.5 Low Energy Electron Microscopy

The fundamental working principle of LEEM is to employ elastically backscattered low energy electrons (up to 100 eV) from the sample surface for imaging its structure, morphology and process dynamics. In the case of a crystalline sample, LEED patterns can be selectively acquired from the surface using a micro aperture. Hence, it is called microbeam LEED (μ-LEED).

4.5.1 The Modes of Operation

Operation modes [126] of the real space imaging are based on contrast mechanisms originated from the amplitude and phase of the electron waves, which upon reflection from the sample produces a diffraction and an amplitude contrast.

Diffraction contrast can be probed in two modes, namely the bright and dark field mode. The bright field mode utilizes normal incidence electron beam to obtain diffracted information from the sample and diffracted intensity around the (0,0) spot is used for imaging. Meanwhile, dark field mode employs off normal incidence beam, which means only surfaces that contribute to the non-zero LEED spots will appear bright. Since reflectivity is dependent on the energy of the incident electron, structures with different symmetries will have different contrasts. This mode is good for distinguishing different rotational domains with the same symmetry in a sample.

The phase contrast mode is based on constructive and destructive interferences of the reflected electrons from the sample surface. Due to the localized phase shifts as a result of the structural differences such as atomic step and number of layers on the surface, these contrasts can be recorded in the image. Therefore, phase contrast is independent of the electron energy.

The mirror mode LEEM is operated by reflecting the incident electrons just above the sample surface so that the electrons are at 0 eV. Therefore the imaging contrast is dependent on the sample work function. This mode is used to study surface dynamics and for alignment of the microscope.

In addition to imaging, it is also possible to record the diffraction patterns. The profound advantage of the μ-LEED method as compared to the macro LEED mentioned in Section 4.4 is that it is feasible to check the surface reconstruction from a selected area down to sub-μm size by utilizing the appropriate aperture.

In this thesis, LEEM is used for studying the *in situ* growth of pentacene molecules on the h-BN nanomesh. With the mirror mode LEEM, the mode and dynamics of the pentacene growth from sub-ML to over 2 ML at RT as well as under thermal influence can be followed in real time. By varying the probing electron energy slightly, it enables the determination of the surface crystallinity, e.g. amorphous or crystalline. Most importantly, μ-LEED is used to identify the different rotational domains of pentacene as a result of its growth on the corrugated nanomesh.

4.5.2 The Equipment

The LEEM setup consists of a series of magnetic lenses for projecting, deflecting, splitting and focusing the beam from the electron gun to the sample and from the sample to the detector, as illustrated by the schematic in Fig. 4.8. A commercial LEEM/PEEM-3 microscope from Elmitec GmbH installed at Beamline I311 at MAX-lab has been used.

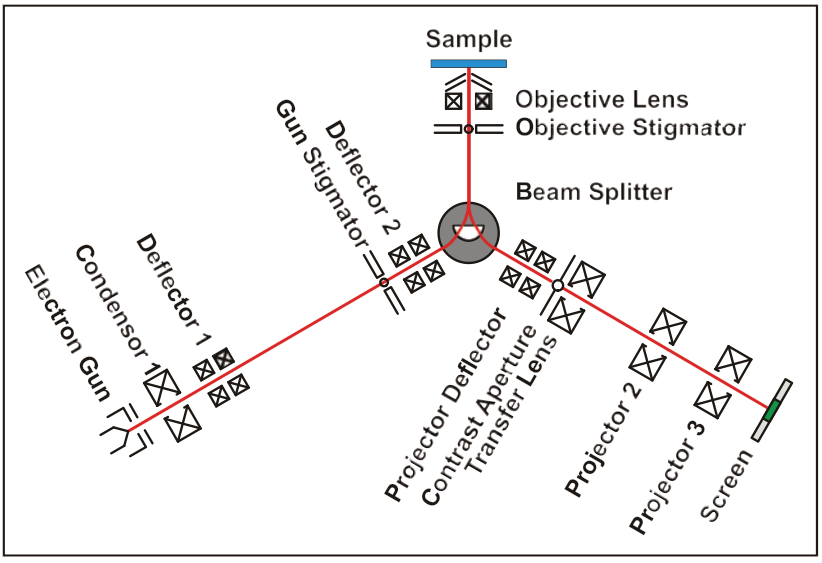

Figure 4.8: An example of the LEEM instrumental setup by ELMITEC GmbH. *Extracted from Heringdorf's presentation entitled "LEEM Basics" in Ref. [126].*

4.6 Scanning Tunneling Microscopy

Electron tunneling phenomenon is a product of quantum mechanics theory, where an electron can be described by a wave function with finite probability of entering a classically forbidden region, i.e. electron can tunnel through the region. The tunneling probability increases exponentially with the decreasing potential barrier width. Therefore the barrier width has to be small enough in order for the tunneling current to be detectable.

STM is a local proximal probing technique and the working concept is based on the fact that electron can tunnel from (to) an atomically sharp metal (normally W) tip to (from) a conducting sample upon application of an appropriate bias voltage between them (typically 1 mV–4 V). The tunneling current (typically 0.1–10 nA) flows from the occupied electronic states near the Fermi level of an electrode into the unoccupied states of the other electrode. Consequently, the current magnitude depends on the tip and surface separation distance and the surface work function. Therefore changes in the current may be due to physical (topography of the surface) and electronic (locally varying work function) properties. With the assistance of a precise piezoelectric drive system to move the tip relative to the sample surface and a current feedback loop, the surface topography can be mapped with atomic resolution under optimized measurement conditions.

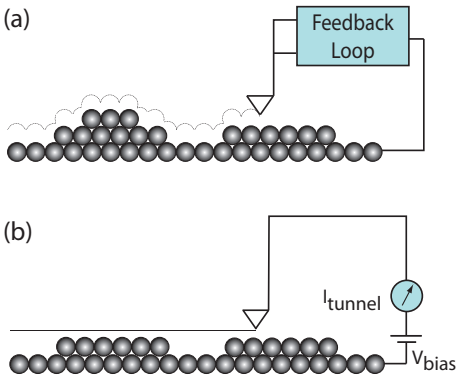

Figure 4.9: Two modes of scanning in STM. (a) Constant current mode applicable for all kinds of conducting surfaces and (b) constant height mode specially for almost atomically flat surfaces.

In general, STM works in two modes of operation, i.e. constant current (most commonly used) as illustrated in Fig. 4.9(a) and constant height modes in Fig. 4.9(b). In the constant current mode, the tunneling current is fixed at a certain value and therefore, the tip is always kept at a constant distance from the sample surface, i.e. it follows the surface structural features. By recording the voltage applied to the piezoelectric driver to keep the tunneling current constant, the height of the tip as a function of its lateral position on the sample is recorded, which can be converted to the surface topographical image. The disadvantage of this mode is the finite response time of the feedback loop and thus the slow scan speed.

On the contrary, the constant height mode scans at a fixed level above the sample surface, i.e. the tip does not follow the surface features. The feedback loop is less sensitive or turned off completely and hence, the fast scan speed is possible. In this mode, the rapidly varying tunneling current containing the topographic information is measured. The obvious advantage here is the fast scanning speed, which can, in turn, reduce image distortions

due to thermal drifts and piezoelectric hysteresis. However, it is difficult to interpret height information from the varying current because the correlation between the distance on the tunneling current is generally not known. Furthermore, this mode is only applicable to atomically flat surfaces because otherwise, the tip may collide with a protruding surface structure.

Despite the wealth of information that STM can offer, the data interpretation is non-trivial. First of all, it is important to differentiate between structural and purely electronic features. In addition, one has to identify real features from artificial effects (caused by multiple tip, blunt tip, etc). A non-ideal tip may cause changes in shape and intensity of the image and consequently it can yield an image very different from the reality. For instance, a defective tip scanning a layer of honeycomb-like graphite can result in a variety of images other than the hexagonal structures, i.e. from arrays of triangles to arrays of ellipses and even linear row-like structures. [127] The tip may also modify the surface simultaneously with the scanning process resulting in artificial images. Thermal drift (surface movement due to fluctuating temperature) is another major problem in STM. Fortunately these problems can be minimized effectively by cooling the sample with liquid helium during scanning. A detailed description on the STM technique is presented in Ref. [127].

5. Summary of Results

A brief synopsis of the published results is given in the following sections. The results demonstrate how a combination of surface techniques can be used to reveal interesting information about the surface and interface systems. Further details are given in the respective papers at the end of this thesis.

5.1 Hexagonal Boron Nitride on Transition Metals

5.1.1 Adsorption and Surface Structure

Previously, the adsorption of h-BN on 3d TMs was investigated by Preobrajenski and co-workers. [9, 10] Here, the impact of the nd-states with higher quantum number, n ($n = 4,5$) on the type and strength of h-BN–TM interaction was investigated in Paper I. For this purpose, a monolayer of h-BN was deposited on two substrates with the same lattice symmetry but different n and electron occupation of the d-band, namely $4d^8$ Rh(111) and $5d^9$ Pt(111). The profiles of the B 1s and N 1s NEXAFS spectra from the h-BN monolayer on Pt(111) were similar to those from bulk h-BN as published in Ref. [9]. Thus, it was concluded that the interaction at the h-BN/Pt interface was very weak (physisorption). In contrast, the π-resonance shoulders, A' and A" from h-BN/Rh(111) were more pronounced, broader and shifted in comparison to those of h-BN/Pt(111) (see Fig. 5.1[red]). This was a clear evidence that the electronic structure of h-BN monolayer on Rh(111) was strongly perturbed and the interaction was chemisorptive. Furthermore, the π-resonance intensities ($\theta = 20°$) of the h-BN/Rh were, in general, lower than those of h-BN/Pt(111). This could be interpreted that there was on average less standing π-states in h-BN/Rh than in h-BN/Pt because the overlayer was rumpled (consisting of pores and wires), which resulted in a mixture of tilted and horizontally orientated π-states.

The angle dependent NEXAFS at the B 1s (Fig. 5.1[left]) and N 1s (Fig. 5.1[right]) edges of these layered systems inferred that the h-BN overlayers were macroscopically flat because the π-resonances (orbitals perpendicular to the overlayer) were most sensitive to the grazing incident photons. However, the h-BN lattice has a slight mismatch with the substrates, i.e. 7.6% for h-BN/Rh and 10.8% for h-BN/Pt. STM images on these systems showed Moiré patterns due to the lattice mismatch (Fig. 2 of Paper I). The mismatch was also visible in the LEED superstructures (Fig. 1 of Paper I). Furthermore, the STM results showed a distinguishable difference in

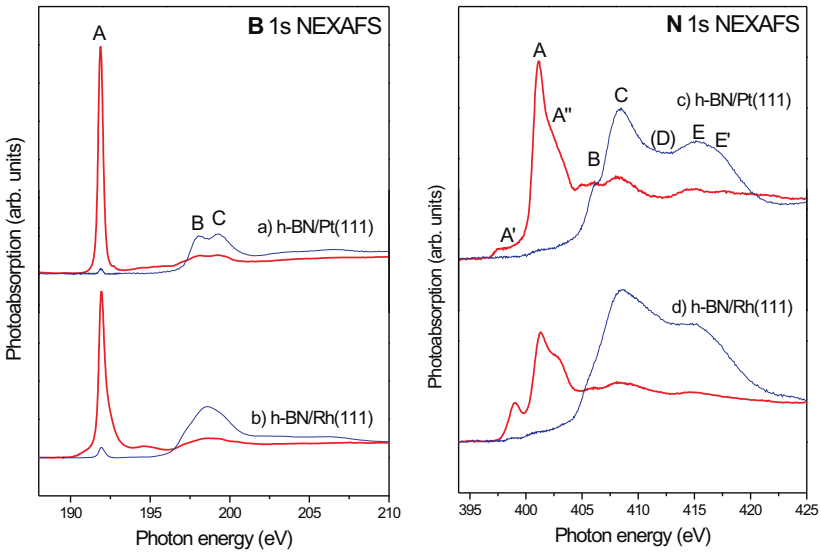

Figure 5.1: Angle dependent NEXAFS at B 1*s* [left] and N 1*s* [right] of h-BN/Pt(111) respective h-BN/Rh(111). Red curves correspond to $\theta = 20^\circ$ and blue curves correspond to $\theta = 90^\circ$, where θ is the angle between the incident photon and the sample surface. Refer to Paper I for the explanations of the labeled features. *From Paper I.*

the chemical environment of the atoms (in this case N) with strongly and weakly bonded sites of h-BN/Rh at a given imaging condition. The micrographs showed sharp resolution on sites with the same electronic state but blurred images on areas with other states. On the other hand, h-BN/Pt gave sharp images throughout the whole surface meaning that the overlayer has an almost uniform electronic state. The only way to explain these results was that the h-BN monolayer on Rh(111) was corrugated but h-BN/Pt(111) was more flat. This could also be deduced from the N 1*s* PE spectra (See Fig. 5 of Paper I) of these systems, which have only one component for h-BN/Pt (nearly flat h-BN) while there were two components with higher binding energies (BEs) for h-BN/Rh (strongly corrugated nanomesh). As a conclusion, the interaction of h-BN with Rh was stronger and the overlayer atoms could exist in two different chemical states, i.e. strongly bound (pores) and weakly bound (wires).

In order to understand the effect of various strengths of the interfacial interaction on the morphology of h-BN/TM, more systematic and comparative studies for systems with gradually evolving substrate electronic configuration (principle quantum number, n and the number of d-electrons) were necessary. Therefore, in Paper II, the substrates were carefully chosen, namely $5d^9$ Pt(111), $5d^8$ Ir(111), $4d^8$ Rh(111) and $4d^7$ Ru(0001) for studying the resulting h-BN surface structure. The NEXAFS at B 1*s* and N 1*s* (Fig. 1 of Paper II) of h-BN on the previously mentioned substrate sequence clearly showed a gradual development of additional structures on both sides of the π-resonances owing to the increasing degree of h-BN π–

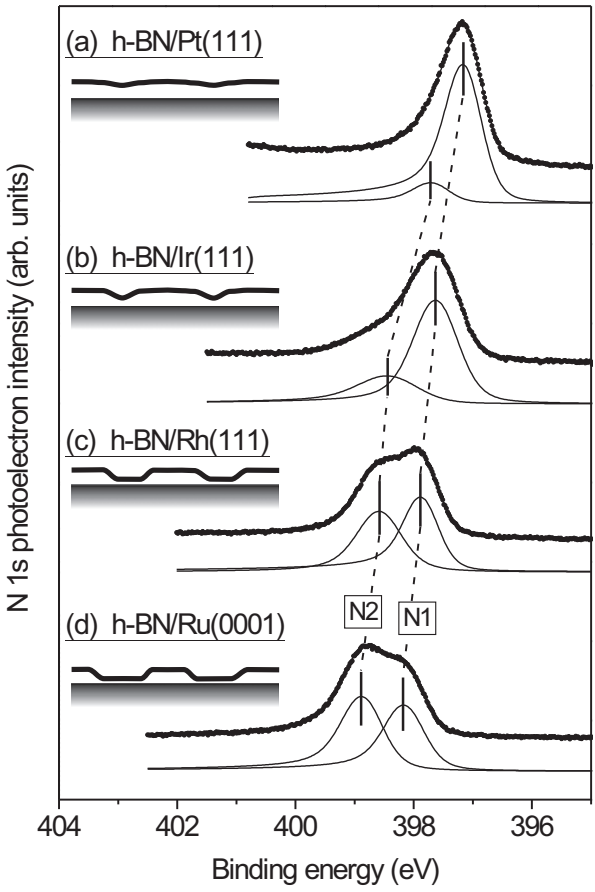

Figure 5.2: N 1*s* PES of (a) h-BN/Pt(111) showing a strong component and a weak shoulder and (b) h-BN/Ir(111) (c) h-BN/Rh(111) and (d) h-BN/Ru(0001) showing two components, namely the non-bonding component, N1 and the bonding one, N2. *From Paper II.*

TM *d* orbital overlap. These structures were attributed to the perturbation of the original electronic structure resulting from the orbital mixing. Similarly, the N 1*s* PES spectra (See Fig. 5.2) of these systems illustrated the increasing strength of interaction. The N 1*s* binding energy increased with increasing interaction. In addition, the gradual appearance of the bonding component (pores) from h-BN/Pt to h-BN/Ru indicated the development of surface corrugation (see the inset schematics of Fig. 5.2).

Beside interfacial interaction and morphology, it was also important to characterize the electronic structure of the adsorbed h-BN layer. It is known that bulk h-BN is an insulator because it has a ~6 eV gap between the valence band and the conduction band. However, the interfacial orbital mixing may result in new h-BN electronic states, which would bridge the band gap making h-BN metallic. The work in paper III was dedicated to the investigation of the gap states of h-BN on metal surfaces. For this purpose, h-BN

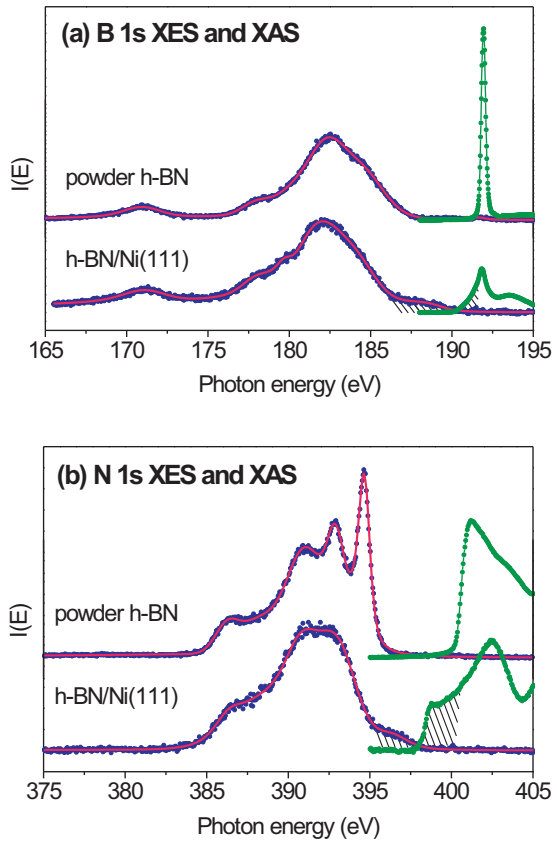

Figure 5.3: XES and XAS of powder h-BN and h-BN/Ni(111) at (a) B 1*s* and (b) N 1*s* showing the appearance of shoulders (new gap states) between the occupied, π and unoccupied, π^* bands upon adsorption on the strongly interacting Ni surface. These states are not visible in the powder h-BN sample. *From Paper III.*

was deposited on three substrates with varying degree of h-BN–TM interaction, namely strong on Ni(111), weak on Pt(111), and a superposition of weakly and strongly bound sites on Rh(111). By combining the NEXAFS and XES results (See Fig. 5.3), it was shown that new gap states (shaded areas) indeed exist in the strongly interacting h-BN/Ni(111) system, which were absent in bulk h-BN. Therefore, it was plausible to conclude that h-BN was partially metallized upon chemisorption on Ni and the degree of metallicity correlated with the strength of interaction.

In order to study the growth processes and to confirm that h-BN on Pt(111) indeed grew as a single atomic layer, microscopic techniques, i.e. STM and LEEM were employed to image its formation in Paper V. The STM images (Fig. 5.4(c-d)) showed only one atomic species in the unit cell while LEEM (Fig. 4 of Paper V) revealed that the number of nucleation sites and the perfection of the growth was strongly dependent on the precursor pressure. These findings together with LEED and NEXAFS results confirmed the model of the nearly flat h-BN monolayer on Pt(111).

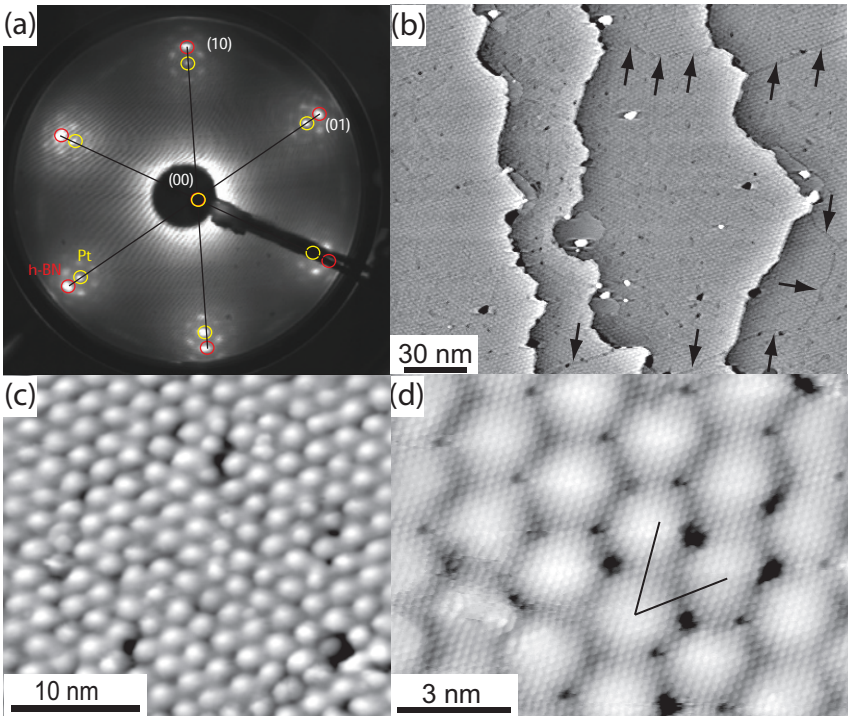

Figure 5.4: (a) LEED pattern displaying the coincidence h-BN layer on Pt(111) surface (red h-BN, yellow Pt(111)). (b) STM image showing areas of the h-BN layer on Pt(111). The arrows indicate domain boundaries. (c) Zoom-in on the h-BN film on Pt(111). (d) STM image displaying atomic resolution. *From Paper V.*

5.1.2 Functionalization of h-BN on TMs

Nanotemplating

The fascinating h-BN nanomesh, which forms exclusively on Rh and Ru, was employed as a template. The attempt to produce Au nanoparticles supported on the h-BN/Rh nanomesh was reported in Paper IV. Furthermore, the influence of temperature on the formation and evolution of Au nanoparticles was also investigated. It was found that Au formed small, mainly 2D nanoparticles on the h-BN/Rh nanomesh but not on the flat h-BN/Pt. On h-BN/Pt, Au formed 3D islands instead. These results were compared to Au deposited on pristine Rh(111) to assure that the nanomesh, not Rh, was indeed responsible for the formation of Au nanoparticles. These samples were characterized by ARPES (Fig. 3 of Paper IV) and Au nanoparticles on the h-BN nanomesh were found to give distinctive, non-dispersive Au 5*d* bands (Fig. 5.5[left]) as opposed to the dispersive bands from Au/Rh (Fig. 3(a) of Paper IV). At room temperature (RT), Au grew in small, nearly 2D islands on the nanomesh (Fig. 5.5[right](a)). Upon annealing between 300 – 500℃, these nanoparticles agglomerated to become larger 3D islands (Fig.

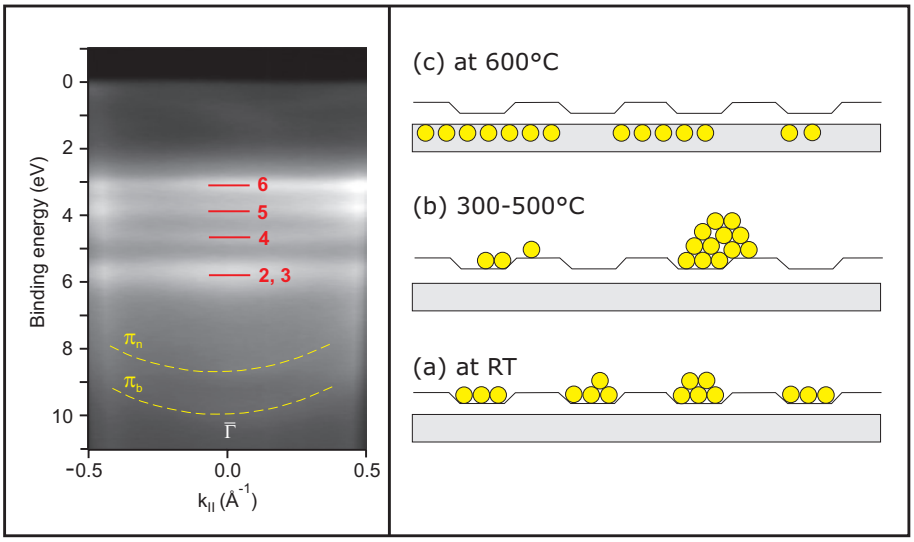

Figure 5.5: [left] ARPES of Au/h-BN/Rh(111) showing the non-dispersive Au 3*d* bands as evidence for well ordered Au nanoparticles. See Paper IV for the description of individual features. [right] Schematics of the Au nanoparticles on the nanomesh (a) at RT, (b) between 300–500°C and (c) at 600°C. *From Paper IV.*

5.5[right](b)). At higher temperatures (about 600°C), Au intercalated through the nanomesh and subsequently, formed a surface alloy with the Rh surface and/or desorbed from the surface (Fig. 5.5[right](c)). These statements agreed with the Au 4*f* PES spectra (Fig. 5 of Paper IV) measured at the respective temperatures. As predicted, the h-BN layer itself stayed structurally intact upon annealing and Au intercalation occured at high temperature, as demonstrated by the N 1*s* NEXAFS (Fig. 7 of Paper IV). This also demonstrated that Au was not residing between h-BN and Rh, which otherwise would result in the spectra similar to those from the bulk h-BN due to the weak Au-BN interaction.

Beside being used as a template, the h-BN nanomesh could also be used for nanostructuring of thin molecular films. This was exemplified by the growth of pentacene (Pn) films on h-BN/Rh in Paper VIII. Pn crystals are known to have excellent electron mobility and thus, they have good potential for the application in organic electronics. In order to understand this interesting system, a comprehensive spectroscopic, microscopic and diffaction studies were performed on the Pn deposited on the corrugated h-BN/Rh. From the micro-LEED results, it was concluded that the corrugated nanomesh has modulated Pn and the Pn overlayer conformed to the nanopatterned surface. Despite this crystal restructuring, the Pn crystal retained its natural herringbone structure, as shown in the STM images in Fig. 5.6(f). From the angle dependent C 1*s* NEXAFS and PES data (Fig. 2 respective 4 of Paper VIII), it was clear that Pn molecules adsorb in the flat lying geometry in the initial state of growth. As more Pn molecules join the

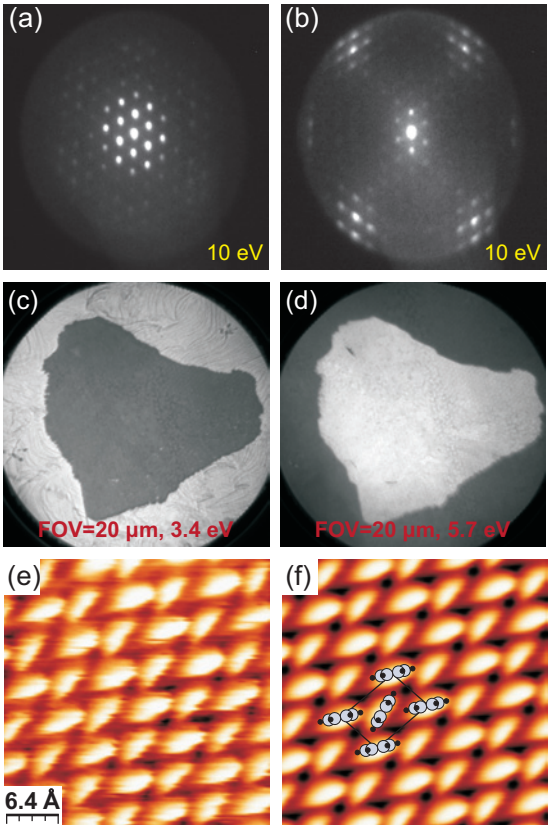

Figure 5.6: [top] (a) Micro-LEED pattern of the clean h-BN nanomesh and (b) one of the Pn domains on the nanomesh. [middle] LEEM images with field of view of 20 µm acquired with the electron energy of (c) 3.4 eV and (d) 5.7 eV. [bottom] (e) STM image of the Pn island on h-BN/Rh and (f) the enhanced image with a schematic of the Pn herringbone crystal structure inserted in the image. *From Paper VIII.*

Pn nucleation centers on the nanomesh, the molecules gained the ability to flip upwards (long side vertically) with the assistance of hydrogen bonds between the neighboring molecules. Eventually, a complete ML of Pn crystal was formed. Micro-LEED (Fig. 5.6[top]) and LEEM (Fig. 5.6[middle]) results confirmed that the crystallinity of Pn was preserved. As a result of the conformation to the nanomesh, several domains of the Pn crystal were found. One of the domains is shown in Fig. 5.6(b). By comparing the adsorption of Pn on the nanomesh and on the highly reactive Rh substrates, it was conclusive that weak interfacial interaction was crucial for the formation of Pn crystal so that the inter-molecule (Pn-Pn) interaction dominated the interfacial interaction (Pn-substrate). However, this was only valid for up to 1 ML of Pn. Above 1 ML, Pn formed large dense islands on the first Pn ML due to DLA, as observed in LEEM. The Pn/h-BN/Rh system was observed to be thermally stable up to 80℃.

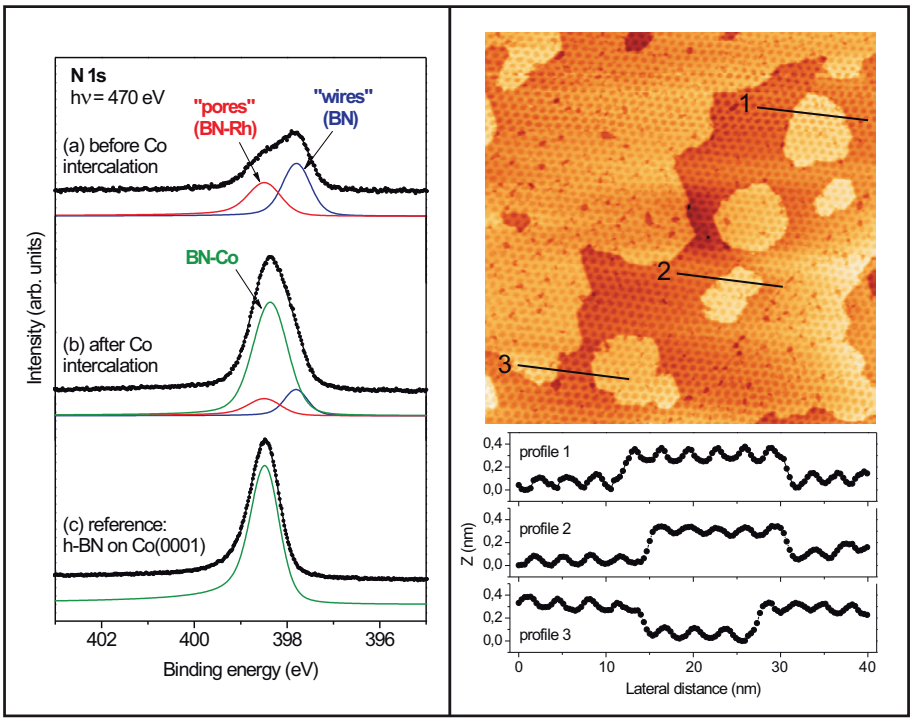

Figure 5.7: [left] PES N 1*s* of Co on h-BN/Rh (a) before and (b) after intercalation as compared to the spectrum from h-BN on Co(0001). [right,top] STM image of the nanomesh with patches (brighter) inflated with intercalated Co and [right,bottom] the respective height profiles of the patches marked with 1, 2 and 3. *From Paper VII.*

It was explained in Sect. 1.4.2 that oxygen can act as a surfactant to reduce the surface free energy of the metal clusters on a surface. From Paper IV, it was known that Au readily formed 2D islands on a Rh surface. Furthermore, Au intercalated easily in the nanomesh upon annealing at 600°C. This was because Au has relatively low surface energy comparing to other transition metals, as estimated in [47]. In Paper VII, it was discovered that Co did not intercalate actively into the nanomesh despite high temperature annealing. Therefore, the concept of oxygen as surfactant to lower the Co surface energy was employed to induce intercalation. Here, co-adsorption of small amount of molecular oxygen with cobalt on h-BN/Rh was studied with PES, NEXAFS, LEED and STM. The spectroscopic and microscopic results (See Fig. 5.7) clearly showed the profound effect of even a tiny amount of O_2 on the Co intercalation. In fact, it only needed soft annealing (450°C) for the initiation of Co intercalation. Since only a small fraction of O_2 was used, the intercalated Co remained metallic, as determined from the NEXAFS spectrum at Co L-edge (Fig. 7(c) of Paper VII). In this way, the intercalation of Co was strictly controlled by the presence of O_2. In fact, the nanomesh remained almost intact upon Co intercalation.

5.2 Graphene on Transition Metals

5.2.1 Adsorption and Surface Structure

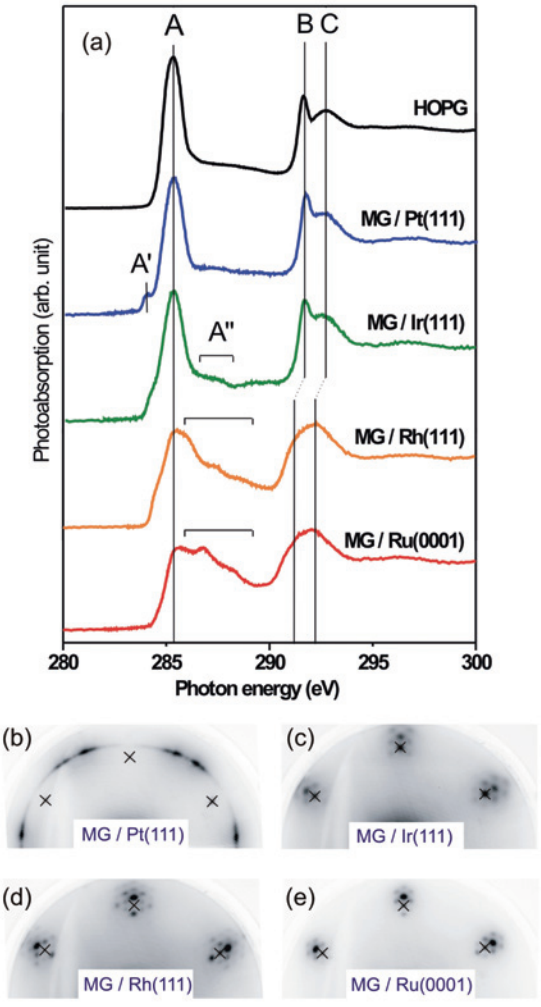

Figure 5.8: (a) C 1*s* NEXAFS of MG on hexagonal faces of Pt, Ir, Rh and Ru. The respective LEED patterns (except HOPG) are shown in (b)–(e). *From Paper VI.*

Due to the many similarities between monolayer h-BN and graphene, it was predicted that both h-BN and graphene would behave similarly upon adsorption on TMs and result in similar overlayer structures. Paper VI reported on the possibility to control graphene corrugation on lattice mismatched TM surfaces. Graphene was deposited on several TM surfaces with varying degree of surface reactivity and lattice constant, namely Pt(111), Ir(111), Rh(111) and Ru(0001) and they were characterized with LEED, C 1*s* NEXAFS, C 1*s* PES and PED. The NEXAFS and PES results were compared to those of highly oriented pyrolytic graphite (HOPG). The B 1*s* NEX-

AFS (Fig. 5.8(a)) of MG on TMs (Pt–Ir–Rh–Ru) showed a gradually increasing change in the shape of the π^*-resonance. The respective LEED superstructures of MG/TM were depicted in Fig. 5.8(b)–(e). The adsorbate reflexes evolved from incommensurate to Moiré-like. The shoulders A' and A" in the C 1*s* NEXAFS, which did not exist for HOPG, became more profound with increasing h-BN-TM interaction. The distinctive feature B and C (σ^*-resonances for HOPG) also became markedly smeared out. It was concluded that MG formed a strongly corrugated overlayer on Rh(111) and Ru(0001), a weakly corrugated overlayer on Ir(111), and a nearly flat overlayer on Pt(111).

5.2.2 Functionalization of MG on TMs

Substrate Catalyzed Reaction

As mentioned earlier in Sect. 1.4.3, TMs are good catalysts for reducing the activation energy of a chemical process. In Paper IX, the experiments were designed to reveal the impact of the TM substrate reactivity on the hydrogenation of graphene on TMs as well as on the hydrogen uptake. The samples were HOPG (not activated by a TM substrate) and MG deposited on TM substrates with increasing reactivity, namely Pt, Ir and Ni. Since molecular hydrogen does not bind to graphene, an atomic H source was used for these experiments. The feasibility of the hydrogenation process was first clarified by the obvious electronic structure changes at the C K-edge of the hydrogenated samples, as shown in Fig. 1 of Paper IX. This was signified by the deficiency of the π^* resonance intensity and the appearance of the C-H peak to the higher energy side of the π^* resonance. The PES C 1*s* spectra of the hydrogenated samples also showed substantial changes. The single-component C 1*s* spectra of HOPG and MG on Ir and Pt became two components for hydrogenated HOPG and three components for the others (Fig. 5.9[left]). The suggested schematic lateral view of the surfaces with increasing atomic buckling due to hydrogenation from HOPG to MG/Ir was portrayed in Fig. 5.9[right]. It was concluded that the H uptake was directly related to the size of the MG-TM bonding sites and it was not proportional to the substrate reactivity. For MG on Pt and Ir, the H adsorption was HOPG-like on the non-bonded sites while graphane-like on the bonded sites between MG and TM. The H uptake was lower on the strongly interacting MG/Ni than on the physisorbed MG/Pt and MG/Ir. It was proposed that only C adsorbed on the on-top sites of Ni may interact with H. For all samples, H adsorption could not occur at the same MG sub-lattice.

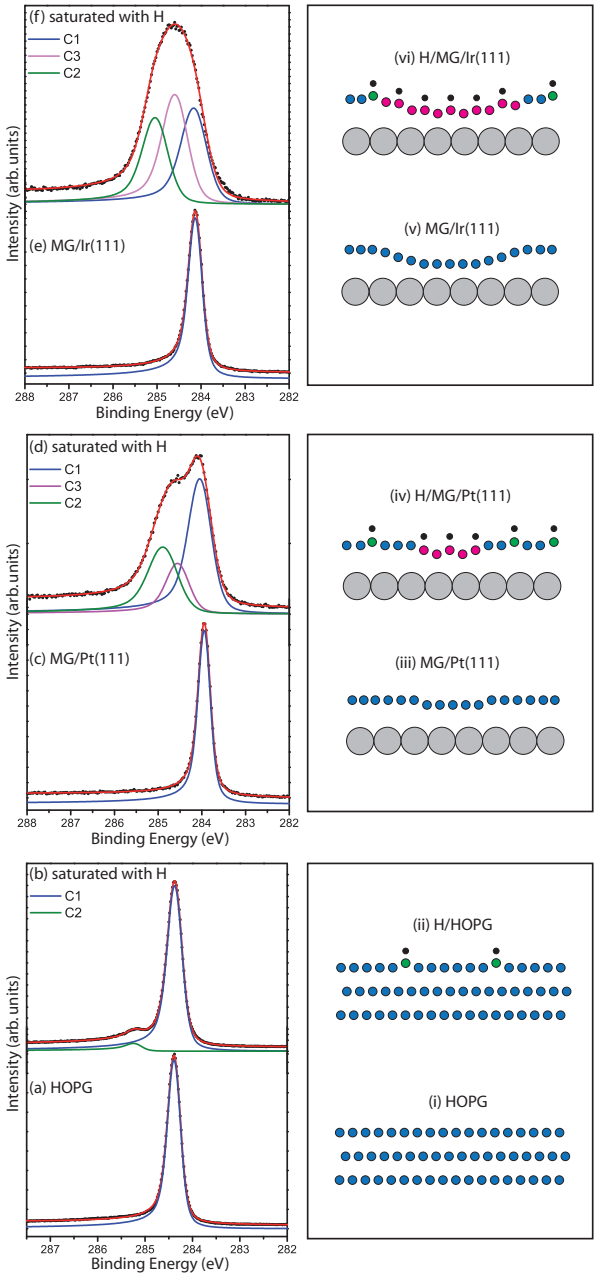

Figure 5.9: [left] PES C 1*s* of the MG/TM samples before and after hydrogenation and [right] their respective schematic diagrams showing the lateral view of the surface. *From Paper IX.*

6. Summary and Outlook

In this thesis a comprehensive understanding of the nature and properties of the h-BN and graphene monolayers on TM surfaces has been gained. Based on this knowledge, it can be concluded that these formidable 2D systems have a considerable potential for practical applications. This is partly because the fabrication of these overlayers by CVD is simple and reproducible. In addition, the process itself is self limiting and it results in well ordered surface structures with high thermal and mechanical stability. Finally, as it has been proven here, these surfaces can be functionalized with a broad spectrum of possibilities.

Virtually, the h-BN and MG monolayers can be decorated with many other metal clusters and chemical functional groups. Metal clusters or nanoparticles are an attractive route to effective catalysis. For example, the well dispersed Au nanoparticles supported on the BN nanomesh could have enhanced catalytic properties. Therefore this system should be investigated in a more realistic catalytic reactor with *in situ* characterization facility such as high pressure PES. In addition to catalysis studies, it is also interesting to study the magnetic properties of other metal clusters supported on these 2D overlayers as well as metal intercalated/embedded in the nanostructured overlayers. This is because periodic arrays of clusters with narrow size distribution can be grown on these substrates, which is the prerequisite for nanomagnetism. For characterization of magnetic properties, magnetic dichroism and hysteresis studies are very promising.

Graphene belongs to the alkene group and can undergo a number of chemical reactions that result in the attachment of different functional groups. These functional groups are the foundation for all organic chemistry reactions. Upon successful surface manipulation with these funcitonal groups, many chemical processes can proceed on these decorated surface. This is important for many applications, e.g. the detection of chemical substances. Through specific chemical bonding, a certain molecules such as proteins and DNA can be attached on these functionalized surface in a controlled manner, which subsequently allows selective imaging and characterization of these molecules. This opens the door to producing chemical detector based on the lab-on-a-chip principle.

7. Populärvetenskaplig Sammanfattning

Mikroskopiska förändringar på ytor av olika material pågår i stort sett obemärkt hela tiden. Alla ytor, speciellt reaktiva metaller, utsätts ständigt av kemiska angrepp med eller utan mänsklig inverkan. Det finns många exempel på detta; från vardagliga företeelser som oxidering av metaller i form av rost och kalkavlagringar i kaffebryggare till mer avancerade som katalytisk omvandling av lågoktanig bensin till den högoktaniga bensin vi tankar våra bilar med. Ett exempel med anknytning till bilar, som förstås är av stort miljöintresse, är nämligen oxidering av kolmonoxid till koldioxid i bilens katalysator.

Atmosfären på jorden består av många olika molekyler och aktiva ämnen. Därför kan flera ytprocesser pågå samtidigt, vilket försvårar bestämningen av processens ursprung och identifieringen av påverkan som kan skynda på eller sakta ner den. För att fullständigt studera och förstå en viss process måste man begränsa den till så få samtidiga kemiska processer som möjligt. Detta görs i vakuumkammare, så inga oönskade molekyler kan påverka det studerade kemiska förloppet. För att få ut informationen kan man använda ytskiktstekniker som elektronspektroskopi och svepspetsmikroskopi.

Varje grundämne i periodiska systemet består bland annat av elektroner som har bestämda bindningsenergier. Därför fungerar bindningsenergin som ett fingeravtryck för ett ämnes kemikaliska tillstånd. Elektronspektroskopi är en metod där man belyser den studerade ytan med röntgenstrålning som är tillräckligt energirik för att vissa elektroner ska kunna lämna ytskiktet. Med hjälp av en analysator försedd med en detektor samlas dessa elektroner upp och ett spektrum visar intensiteten för olika bindningsenergier. Ett sådant spektrum kan jämföras med regnbågen där varje färg motsvarar en bindningsenergi och ljusstyrkan motsvarar antalet elektroner som fångas upp.

Med svepspetsmikroskopi kan man skapa en bild över den studerade ytan likt fotografi. Skillnaden är att istället för ljus som fångas upp av den ljuskänsliga detektoren i kameran så är det elektroner som samlas upp i en väldigt spetsig nål i mikroskopet. Nålen sveps fram över ytan samtidigt som den samlar upp elektroner. Elektroner på olika avstånd från nålen representeras av olika ljusstyrka i bilden. Därmed skapas en bild över det undersökta området, vilken visar ytans topografi.

Genom att kombinera spektroskopi med mikroskopi i ytskiktsstudier kan man skapa både en översiktsbild i form av ett energispektrum och en närbild (helst med atomär upplösning) av den undersökta ytan. Detta underlättar tolkningen av resultaten, t.ex. kan en topp som dyker upp i spek-

tret bero på ett kemikaliskt eller fysikaliskt tillstånd. Tillsammans med en mikroskopisk bild är det lättare att avgöra vilket.

Denna avhandling handlar om att studera egenskaperna hos atomärt tunna skikt av bornitrid respektiv grafen (tunn grafit) på ett underlag av olika övergångsmetaller med hjälp av elektronspektroskopi och svepspetsmikroskopi. De studerade ytorna bildar mikrostrukturer p.g.a. växelverkan med metallen i underlaget och kan därmed bl.a. fungera som en mall för att fånga upp molekyler och metallkluster (ett kluster består av mellan 10–100 atomer) enligt ett visst mönster. Dessa typer av självorganiserade ytskiktssytem är mycket intressanta och har stor betydelse för både grundforskning såsom teknologiutveckling. Möjliga användningsområden är framställning av elektronikkomponenter, detektorer och katalysatorer.

8. Acknowledgment

It took four years of intensive learning and explorative adventure to produce this final piece of work. Through the years, there were many good moments and there were also several not so good ones during the endeavor. All in all, this doctoral experience has enriched as well as transformed my life enormously. To my surprise, I have actually exceeded my own expectations. However, at times, things were really testing the limit of my patience and even my sanity. But somehow I managed to pull through such unfortunate situations without completely losing my mind thanks to the kind and supportive people around me. Without the following people, this work would not have been possible. In fact, it is hardly even imaginable.

First and foremost, I wish to extend my heartfelt gratitude to my thesis supervisors, Prof. Nils Mårtensson and Dr. Alexei Preobrajenski. Nils has been very supportive and giving me the freedom to steer the direction of my work. I especially appreciate that he has always been able to reserve his time to attend to my work despite his tight schedule. Alexei is the mastermind of this work. As a leader, I admire his intelligence, quick-wittedness and creative thinking. As a friend, he is humble, kind and caring. I thank both of you for this invaluable opportunity to work with you. I have really enjoyed this work as well as working with you.

I have met many people in my life. But some of them are especially significant because they have given me the precious chance to continue on a career of my choice in Physics. For this, I sincerely thank Prof. Harry Whitlow and Prof. Herbert Moser for believing in me when very few did. Without you, I would have lost my chance in this interesting career.

The achievements in this dissertation is not solely mine. With honor, I dedicate this final piece of work to all my friends, colleagues and collaborators from MAX-lab, Uppsala University, Lund University, Dublin City University, St. Petersburg State University and Linköping University. Nevertheless, I would also like to thank the administration team at Uppsala University and MAX-lab for taking care of the financial matters and for assisting me with the administrative works.

I am grateful for all my friends from all around the world. Thank you for brightening up my day when things are getting a bit too harsh, for being there for me (often virtually these days) when I need you as well as for sharing my (often non-work related) interests. Cheers to all of you!

It can be very lonely sometimes to be away from my native home. I consider myself lucky because I have a "surrogate" family in Sweden. A special

thank to the Aldenius and Jönsson for being my family and for taking very good care of me.

Peter, there is no thank in the entire world that is enough to express my appreciation and gratefulness for all you have done and are still doing for me. You have the patience of an angel.

Lastly but importantly, I wish to thank my parents, May Cheng and family and May Sum for your love. Although I am faraway from the family, you are always close to me in my heart.

Bibliography

[1] T. Ando, A. B. Fowler, and F. Stern. Electronic properties of two-dimensional systems. *Reviews of Modern Physics*, 1982, 54(2),437.

[2] C. Oshima and A. Nagashima. Ultra-thin epitaxial films of graphite and hexagonal boron nitride on solid surfaces. *Journal of Physics: Condensed Matter*, 1997, 9,1–20.

[3] L. Pauling. *The nature of chemical bonds*. Cornell University Press, 1960.

[4] R. T. Paine and C. K. Narula. Synthetic routes to boron nitride. *Chemical Reviews*, 1990, 90(1).

[5] M. T. Paffett, R. J. Simonson, P. Papin, and R. T. Paine. Borazine adsorption and decomposition at Pt(111) and Ru(0001) surfaces. *Surface Science*, 1990, 232,286–296.

[6] A. Nagashima, N. Tejima, Y. Gamou, T. Kawai, and C. Oshima. Electronic structure of monolayer hexagonal boron nitride physisorbed on metal surfaces. *Physical Review Letters*, 1995, 75(21),3918.

[7] E. Rokuta, Y. Hasegawa, K. Suzuki, Y. Gamou, C. Oshima, and A. Nagashima. Phonon dispersion of an epitaxial monolayer film of hexagonal boron nitride on Ni(111). *Physical Review Letters*, 1997, 79(23).

[8] M. Corso, W. Auwärter, M. Muntwiller, A. Tamai, T. Greber, and J. Osterwalder. Boron nitride nanomesh. *Science*, 2004, 303(217).

[9] A. B. Preobrajenski, A. S. Vinogradov, and N. Mårtensson. Ni $3d$–BN π hybridization at the h-BN/Ni(111) interface observed with core-level spectroscopies. *Physical Review B*, 2004, 70(165404).

[10] A. B. Preobrajenski, A. S. Vinogradov, and N. Mårtensson. Monolayer of h-BN chemisorbed on Cu(111) and Ni(111): The role of the transition metal $3d$ states. *Journal of Surface Science*, 2005, 306,666.

[11] J. Wintterlin and M. L. Bocquet. Graphene on metal surfaces. *Journal of Surface Science*, 2009, 603,1841–1852.

[12] A. K. Geim and K. S. Novoselov. The rise of graphene. *Nature Materials*, 2007, 6,183.

[13] K. S. Novoselov, D. Jiang, F. Schedin, T. J. Booth, V. V. Khotkevich, S. V. Morozov, and A. K. Geim. Two-dimensional atomic crystals. *Proceedings of the National Academy of Sciences*, 2005, 102(30),10451–10453.

[14] N. R. Gall', E. V. Rut'kov, and A. Y. Tontegode. Two dimensional graphite films on metals and their intercalation. *Internationl Journal of Modern Physics B*, 1997, 11(16),1865–1911.

[15] D. Pacilé, J. C. Meyer, Ç. Ö. Girit, and A. Zettl. The two-dimensional phase of boron nitride: Few-atomic-layer sheets and suspended membranes. *Applied Physics Letters*, 2008, 92(133107).

[16] A. K. Geim. Graphene: Status and prospects. *Science*, 2009, 324,1530–1534.

[17] S. Berner, M. Corso, R. Widmer, O. Groening, R. Laskowski, P. Blaha, K. Schwarz, A. Goriachko, H. Over, S. Gsell, M. Schreck, H. Sachdev, T. Greber, and J. Osterwalder. Boron nitride nanomesh: Functionality from a corrugated monolayer. *Angewandte Chemie*, 2007, 46,5115–5119.

[18] D. W. Boukhvalov, M. I. Katsnelson, and A. I. Lichtenstein. Hydrogen on graphene: Electronic structure, total energy, structural distortions and magnetism from first-principles calculations. *Physical Review B*, 2008, 77(035427).

[19] M. Haruta, N. Yamada, T. Kobayashi, and S. Iijima. Gold catalyst prepared by coprecipitation for low-temperature oxidation of hydrogen and of carbon monoxide. *Journal of Catalysis*, 1989, 115,301–309.

[20] M. Haruta. Catalysis and applications of gold nanoparticles. *Studies in Surface Science and Catalysis*, 2003, 145,31–38.

[21] K. W. Kolasinski. *Surface Science: Foundations of Catalysis and Nanoscience*. John Wiley and Sons, 2008.

[22] A. C. Luntz. *Chemical Bonding at Surfaces and Interfaces*. Elsevier B. V., 2008.

[23] I. Chorkendorff and J. W. Niemantsverdriet. *Concepts of modern catalysis and kinetics*. Wiley-VCH Verlag GmbH, 2003.

[24] R. Smoluchowski. Anisotropy of the electronic work function of metals. *Physical Review*, 1941, 60,661.

[25] G. M. Whitesides and B. Grzybowski. Self-assembly at all scales. *Science*, 2002, 295,2418.

[26] G. M. Whitesides and M. Boncheva. Beyond molecules: Self assembly of mesoscopic and macroscopic components. *Proceedings of the National Academy of Sciences*, 2002, 99(8),4769.

[27] T. T. Magkoev, A. M. Turiev, N. I. Tsideva, D. G. Panteleev, G. G. Vladimirov, and G. A. Rump. Adsorption of boron on a Mo(110) surface. *Journal of Physics: Condensed Matter*, 2008, 20(48),485007.

[28] A. N. MacInnes, A. R. Barron, J. J. Li, and T. R. Gilbert. Reaction bonded refractory metal carbide/carbon composites. *Polyhedron*, 1994, 13(8),1315.

[29] C. T. Campbell, D. C. Foyt, and J. M. White. Oxygen penetration into the bulk of palladium. *Journal of Physical Chemistry*, 1977, 81(5),491.

[30] C. W. Bauschlicher. The coverage-dependent effect on the barrier for oxyen penetration into a metal lattice. *Chemical Physics Letters*, 1985, 118(6).

[31] P. K. Stefanov and T. S. Marinova. HREELS study of the interaction of oxygen with a Mo(111) surface. *Surface Science*, 1988, 200(1),26.

[32] N. T. Barrett, R. Belkhou, J. Thiele, and C. Guillot. A core-level photoemission spectroscopy study of the formation of surface alloy Cu/Pt(111): comparison with Pt/Cu(111). *Surface Science*, 1995, 331-333,776–781.

[33] E. Bauer and H. Poppa. Recent advances in epitaxy. *Thin Solid Films*, 1972, 12,167–185.

[34] C. Argile and G. E. Rhead. Adsorbed layer and thin film growth modes monitored by auger electron spectroscopy. *Surface Science Reports*, 1989, 10,277–356.

[35] T. A. Witten and L. M. Sander. Diffusion-limited aggregation: A kinetic critical phenomenon. *Physical Review Letter*, 1981, 47(19),1400.

[36] T. A. Witten and L. M. Sander. Diffusion-limited aggregation. *Physical Review B*, 1983, 27(5686).

[37] J. W. Evans. Analysis of a diffusion-limited island growth mechanism for chemisorption and epitaxy. *Physical Review A*, 1989, 40(5),2868–2870.

[38] R. Schlögl, G. Ertl, H. Knözinger, F. Schüth, and J. Weitkamp. *Handbook of Heterogeneous Catalysis*, volume 1. Wiley VCH, 2008.

[39] J. A. Moulijn, A. E. van Diepen, F. Kapteijn, G. Ertl, H. Knözinger, F. Schüth, and J. Weitkamp. *Handbook of Heterogeneous Catalysis*, volume 4. Wiley VCH, 2008.

[40] www.wikipedia.org.

[41] A. Savara, C. M. Schmidt, F. M. Geiger, and E. Weitz. Adsorption entropies and enthalpies and their implications for adsorbate dynamics. *Journal of Physical Chemistry*, 2009, 113,2806–2815.

[42] R. P. Feynman's talk, www.zyvex.com/nanotech/feynman.html.

[43] N. R. Gall', E. V. Rut'kov, A. Y. Tontegode, and M. M. Usufov. Intercalatoin of two-dimensional graphite films on metals by atoms and molecules. *Technical Physics*, 1999, 40(9),1066.

[44] A. Nagashima, N. Tejima, and C. Oshima. Electronic states of the pristine and alkali-metal-intercalated monolayer graphite/Ni(111) systems. *Physical Review B*, 1994, 50(23),17487.

[45] P. A. Khomyakov, G. Giovannetti, P. C. Rusu, G. Brocks, J. van den Brink, and P. J. Kelly. First-principles study of the interaction and charge transfer between graphene and metals. *arXiv:0902.1203v1*, 2009.

[46] N. A. Kholin, E. V. Rut'kov, and A. Y. Tontegode. The nature of the adsorption bond between graphite islands and iridium surface. *Surface Science*, 1984, 139,155–172.

[47] L. Vitos, A. V. Ruban, H. L. Skriver, and J. Kollár. The surface energy of metals. *Surface Science*, 1998, 80,186.

[48] C. Tölkes, R. Struck, R. David, P. Zeppenfield, and G. Comsa. Surfactant-induced layer-by-layer growth on a highly anisotropic substrate: Co/Cu(110). *Physical Review Letter*, 1998, 80(13),2877.

[49] E. A. Heintz and W. E. Parker. Catalytic effect of major impurities on graphite oxidation. *Carbon*, 1966, 4(4),473–482.

[50] H. P. Bonzel and H. J. Krebs. Surface science approach to heterogeneous catalysis: CO hydrogenation on transition metals. *Surface Science*, 1982, 117,639–658.

[51] R. M. Martin. *Electronic structure: Basic theory and practical methods*. Cambridge University Press, 2005.

[52] W. A. Harrison. *Electronic structure and the properties of solids*. Dover Publications, Inc., New York, 1989.

[53] E. Kaxiras. *Atomic and electronic structure of solids*. Cambridge University Press, 2003.

[54] J. H. Davies. *The Physics of low-dimensional semiconductors: An introduction*. Cambridge University Press, 2005.

[55] wiki.fysik.dtu.dk/gpaw.

[56] www.pi5.uni-stuttgart.de/agnomt/research/oscillatorstrength/lds.html.

[57] V. Grasso, editor. *Electronic structure and electronic transitions in layered materials*. Series A: Layered Structures. D. Reidel Publishing Company, 1986.

[58] P. R. Wallace. The band theory of graphite. *Physical Review*, 1947, 71(9),622.

[59] S. Reich, J. Maultzsch, C. Thomsen, and P. Ordejón. Tight-binding description of graphene. *Physical Review B*, 2002, 66(035412).

[60] A. Castellani, M. Posternak, and A. Baldereschi. Bulk and surface electronic structure of hexagonal boron nitride. *Physical Review B*, 1987, 36(11),6105.

[61] N. Ooi, A. Rairkar, L. Lindsley, and J. B. Adams. Electronic structure and bonding in hexagonal boron nitride. *Journal of Physics: Condensed Matter*, 2006, 18(1),97.

[62] N. Ooi, A. Rairkar, L. Lindsley, and J. B. Adams. Density functional study of graphite bulk and surface properties. *Carbon*, 2006, 44,231.

[63] M. S. Fuhrer, C. N. Lau, and A. H. MacDonald. Graphene: Materially better carbon. *MRS Bulletin*, 2010, 35,289.

[64] T. Ohta, A. Bostwick, T. Seyller, K. Horn, and E. Rotenberg. Controlling the electronic structure of bilayer graphene. *Science*, 2006, 313,951.

[65] www.nextnano.de.

[66] Y. W. Son, M. L. Cohen, and S. G. Louie. Energy gaps in graphene nanoribbons. *Physical Review Letter*, 2006, 97(216803).

[67] Y. W. Son, M. L. Cohen, and S. G. Louie. Half-metallic graphene nanoribbons. *Nature*, 2006, 444(7117),347.

[68] R. M. Ribeiro, N. M. R. Peres, J. Coutinho, and P. R. Briddon. Inducing energy gaps in monolayer and bilayer graphene: Local density approximation calculations. *Physical Review B*, 2008, 78(075442).

[69] R. E. Watson, M. L. Perlman, and J. F. Herbst. Core level shifts in the 3d transition metals and tin. *Physical Review B*, 1976, 13(6),2358.

[70] N. Mårtensson and A. Nilsson. *Applications of synchrotron radiation, High-resolution core-level photoemission spectroscopy of surfaces and absorbates*. Springer Series in Surface Sciences 35. Springer-Verlag, 1995.

[71] B. Johansson and N. Mårtensson. Theory of surface core-level binding energy shifts in metals. *Helvetica Physica Acta*, 1983, 56,405.

[72] B. Johansson and N. Mårtensson. Core-level binding energy shifts for the metallic elements. *Physical Review B*, 1980, 21(10),4427.

[73] J. N. Andersen, D. Hennig, M. Methfessel, R. Nyholm, and M. Scheffler. Surface core level shifts of some 4d-metal single-crystal surfaces; experiments and *ab initio* calculations. *Physical Review B*, 1994, 50(23),17525.

[74] A. S. Y. Chan, G. K. Wertheim, H. Wang, M. D. Ulrich, J. E. Rowe, and T. E. Madey. Surface atom core-level shifts of clean and oxygen-covered Re(12$\bar{3}$1). *Physical Review B*, 2005, 72(035442).

[75] N. Mårtensson, H. B. Saalfeld, H. Kuhlenbeck, and M. Neumann. Structural dependence of the 5d-metal surface energies as deduced from surface core-level shift measurements. *Physical Review B*, 1989, 39(12),8181.

[76] M. Weinert, J. W. Davenport, and R. E. Watson. Final-state screening of core holes in metals. *Physical Review B*, 1986, 34(4),2971.

[77] J. F. van der Veen, F. J. Himpsel, and D. E. Eastman. Structural-dependent 4f core-level binding energies for surface atoms on Ir(111), Ir(100), Ir(100)-(5 x 1) and metastable Ir(100)-(1 x 1). *Physical Review Letters*, 1980, 44(3),189.

[78] G. A. Somorjai. *Introduction to Surface Chemistry and Catalysis*. John Wiley and Sons, 1994.

[79] R. Laskowski and P. Blaha. *Ab initio* study of h-BN nanomeshes on Ru, Rh and Pt. *Physical Review B*, 2010, 81(075418).

[80] S. Lizzit, A. Baraldi, A. Grosso, K. Reuter, M. V. Ganduglia-Pirovano, C. Stampfl, M. Scheffler, M. Stichler, C. Keller, W. Wurth, and D. Menzel. Surface core-level shifts of clean and oxygen-covered Ru(0001). *Physical Review B*, 2001, 63(205419).

[81] S. Lizzit, Y. Zhang, K. L. Kostov, L. Petaccia, A. Baraldi, D. Menzel, and K. Reuter. O- and H-induced surface core level shifts on Ru(0001): prevalence of the additivity rule. *Journal of Physics: Condensed Matter*, 2009, 21,134009.

[82] M. V. Ganduglia-Pirovano, M. Scheffler, A. Baraldi, S. Lizzit, G. Comelli, G. Paolucci, and R. Rosei. Oxygen-induced Rh $3d_{5/2}$ surface core-level shifts on Rh(111). *Physical Review B*, 2001, 63(205415).

[83] K. Dücker, K. C. Prince, H. P. Bonzel, V. Cháib, and K. Horn. Adsorption-induced surface core-level shifts in Pt(110). *Physical Review B*, 1987, 36(12),6292.

[84] C. Puglia, A. Nilsson, B. Hernnäs, O. Karis, P. Bennich, and N. Mårtensson. Physisorbed, chemisorbed and dissociated O_2 on Pt(111) studied by different core level spectroscopy methods. *Surface Science*, 1995, 342,119.

[85] M. Bianchi, D. Cassese, A. Cavallin, R. Comin, F. Orlando, L. Postregna, E. Golfetto, S. Lizzit, and A. Baraldi. Surface core level shifts of clean and oxygen covered Ir(111). *New Journal of Physics*, 2009, 11(063002).

[86] M. Basche and D. Schiff. New pyrolitic boron nitride. *Materials in Design Engineering*, 1964, page 78.

[87] H. O. Pierson. Boron nitride composite by chemical vapor deposition. *Journal of Composite Materials*, 1975, 9,228.

[88] N. J. Archer. *Chemical Society (London) Special Publication*, 1977, 30,167.

[89] R. Laskowski, P. Blaha, T. Gallauner, and K. Schwarz. Single layer model of the hexagonal boron nitride nanomesh on the Rh(111) surface. *Physical Review Letters*, 2007, 98(106802).

[90] O. Bunk, M. Corso, D. Martoccia, R. Herger, P. R. Willmott, B. D. Patterson, J. Osterwalder, J. F. van der Veen, and T. Greber. Surface x-ray diffraction study of boron nitride nanomesh in air. *Surface Science*, 2007, 601,L7–L10.

[91] R. Laskowski and P. Blaha. Unraveling the structure of the h-BN/Rh(111) nanomesh with *ab initio* calculations. *Journal of Physics: Condensed Matter*, 2008, 20(064207).

[92] A. Goriachko, Y. He, M. Knapp, and H. Over. Self-assembly of a hexagonal boron nitride nanomesh on Ru(0001). *Langmuir*, 2007, 23,2928–2931.

[93] W. Auwärter, M. Muntwiler, T. Greber, and J. Osterwalder. Co on h-BN/Ni(111): from island to island-chain formation and co intercalation. *Surface Science*, 2002, 511,379.

[94] A. Goriachko, Y. B. He, and H. Over. Complex growth of NanoAu on BN nanomesh supported by Ru(0001). *Journal Physical Chemistry C*, 2008, 112(22),8147.

[95] J. Zhang, V. Sessi, C. H. Michaelis, I. Brihuega, J. Honolka, K. Kern, R. Skomski, X. Chen, G. Rojas, and A. Enders. Ordered layers of Co clusters on BN template layers. *Physical Review B*, 2008, 78(165430).

[96] W. Auwärter, T. J. Kreutz, T. Greber, and J. Osterwalder. XPD and STM investigation of hexagonal boron nitride on Ni(111). *Surface Science*, 1999, 429,229.

[97] M. Morscher, M. Corso, T. Greber, and J. Osterwalder. Formation of single layer h-BN on Pd(111). *Surface Science*, 2006, 600,3280.

[98] F. Müller, K. Stöwe, and H. Sachdev. Symmetry versus commensurability: Epitaxial growth of hexagonal boron nitride on Pt(111) from b-trichloroborazine $(ClBNH)_3$. *Chemistry of Materials*, 2005, 17(13),3464.

[99] W. M. Hess and L. L. Ban. *Proc. 6th Int. Congr. on Electron Microscope (Kyoto)*, 1966, 1,569.

[100] A. E. Karu and M. Beer. Pyrolytic formation of highly crystalline graphite films. *Journal of Applied Physics*, 1966, 37(2179).

[101] B. Lang. A LEED study of the deposition of carbon on platinum crystal surfaces. *Surface Science*, 1975, 53,317–329.

[102] A. Nagashima. Ph.D thesis, Waseda University, 1995.

[103] Y. Gamo, A. Nagashima, M. Wakabayashi, M. Terai, and C. Oshima. Atomic structure of monolayer graphite formed on Ni(111). *Surface Science*, 1997, 374,61–64.

[104] A. M. Shikin, D. Farias, V. K. Adamchuk, and K. H. Rieder. Surface phonon dispersion of a graphite monolayer adsorbed on Ni(111) and its modification caused by intercalation of Yb, La and Cu layers. *Surface Science*, 1999, 424,155–167.

[105] J. Algdal, T. Balasubramanian, M. Breitholtz, T. Kihlgren, and L. Walldén. Thin graphite overlayers: Graphene and alkali metal intercalation. *Surface Science*, 2007, 601,1167–1175.

[106] A. T. N'Diaye, S. Bleikamp, P. J. Feibelman, and T. Michely. Two-dimensional Ir cluster lattice on a graphene Moiré on Ir(111). *Physical Review Letters*, 2006, 97(215501).

[107] W. Moritz, B. Wang, M. L. Bocquet, T. Brugger, T. Greber, J. Wintterlin, and S. Günther. Structure determination of the coincidence phase of graphene on Ru(0001). *Physical Review Letters*, 2010, 104(136102).

[108] T. Brugger, S. Günther, B. Wang, J. H. Dil, M.-L. Bocquet, J. Osterwalder, J. Wintterlin, and T. Greber. Comparison of electronic structure and template function of single-layer graphene and a hexagonal boron nitride nanomesh on Ru(0001). *Physical Review B*, 2009, 79(045407).

[109] D. Martoccia, P. R. Willmott, T. Brugger, M. Björck, S. Günther, C. M. Schlepütz, A. Cervellino, S. A. Pauli, B. D. Patterson, S. Marchini, J. Wintterlin, W. Moritz, and T. Greber. Graphene on Ru(0001): A 25×25 supercell. *Physical Review Letters*, 2008, 101(126102).

[110] D. Martoccia, M. Björck, C. M. Schlepütz, T. Brugger, S. A. Pauli, B. D. Patterson, T. Greber, and P. R. Willmott. Graphene on Ru(0001): a corrugated and chiral structure. *New Journal of Physics*, 2010, 12(043028).

[111] V. M. Karpan, G. Giovannetti, P. A. Khomyakov, M. Talanana, A. A. Starikov, M. Zwierzycki, and J. van den Brink. Graphite and graphene as perfect spin filters. *Physical Review Letters*, 2007, 99(176602).

[112] G. Giovannetti, P. A. Khomyakov, G. Brocks, P. J. Kelly, and J. van den Brink. Substrate-induced band gap in graphene on hexagonal boron nitride: *Ab initio* density functional calculations. *Physical Review B*, 2007, 76(073103).

[113] X. Li, W. Cai, J. An, S. Kim, J. Nah, D. Yang, R. Piner, A. Velamakanni, I. Jung, E. Tutuc, S. K. Banerjee, L. Colombo, and R. S. Ruoff. Large-area syntheis of high quality and uniform graphene films on copper foils. *Science*, 2009, 324,1312–1214.

[114] L. Gao, J. R. Guest, and N. P. Guisinger. Epitaxial graphene on Cu(111). *Nano Letters*, 2010, Article ASAP.

[115] C. N. Berglund and W. E. Spicer. Photoemission studies of copper and silver: Theory and experiment. *Physical Review*, 1964, 136(4A),1030.

[116] A. B. Preobrajenski. *Ultrathin semiconductor layers on InP(110) and InP(001): some unusual interfaces*. Ph.D thesis, Department of Chemistry and Mineralogy, Leipzig University, 2001.

[117] N. Mårtensson, R. Nyholm, and B. Johansson. Four-hole satellites in the L_3VV auger and the valence-band spectra from nickel. *Physical Review B*, 1984, 30(4),2245–2248.

[118] S. Hüfner and G. K. Wertheim. Multielectron effects in the XPS spectra of nickel. *Physical Letters*, 1975, 51A(5),299–300.

[119] S. Doniach and M. Šunjić. Many-electron singularity in x-ray photoemission and x-ray line spectra from metals. *Journal of Physics C: Solid State Physics*, 1970, page 285.

[120] S. Hüfner and G. K. Wertheim. Core-line asymmetries in the x-ray photoemission spectra of metals. *Physical Review B*, 1975, 11(2),678.

[121] A. M. Bradshaw and D. P. Woodruff. *Structure determination of molecular adsorbates using photoelectron diffraction*. Springer Series in Surface Sciences 35. Springer-Verlag, 1995.

[122] S. Hüfner. *Photoelectron Spectroscopy: Principles and Applications, 3rd Edition*. Springer-Verlag, 2003.

[123] VG Scienta, www.vgscienta.com.

[124] J. Stöhr. *NEXAFS Spectroscopy*. Springer Series in Surface Sciences 25. Springer-Verlag, 2003.

[125] M. A. V. Hove and W. H. W. adn C M Chang. *Low-Energy Electron Diffraction: Experiment, Theory and Surface Structure Determination*. Springer Series in Surface Sciences 6. Springer Verlag, 1986.

[126] www.leem-user.com.

[127] H.-J. Güntherodt and R. Wiesendanger. *Scanning Tunneling Microscopy I*. Springer-Verlag, 1992.

Acta Universitatis Upsaliensis

Digital Comprehensive Summaries of Uppsala Dissertations from the Faculty of Science and Technology 766

Editor: The Dean of the Faculty of Science and Technology

A doctoral dissertation from the Faculty of Science and Technology, Uppsala University, is usually a summary of a number of papers. A few copies of the complete dissertation are kept at major Swedish research libraries, while the summary alone is distributed internationally through the series Digital Comprehensive Summaries of Uppsala Dissertations from the Faculty of Science and Technology. (Prior to January, 2005, the series was published under the title "Comprehensive Summaries of Uppsala Dissertations from the Faculty of Science and Technology".)

Distribution: publications.uu.se
urn:nbn:se:uu:diva-130342

ACTA
UNIVERSITATIS
UPSALIENSIS
UPPSALA
2010